Comparison of the Quaternary travertine sites in the Denizli extensional basin based on their depositional and geochemical data

Mehmet Özkul [a,*], Sándor Kele [b], Ali Gökgöz [a], Chuan-Chou Shen [c], Brian Jones [d], Mehmet Oruç Baykara [a], István Fórizs [b], Tibor Németh [b], Yu-Wei Chang [c], Mehmet Cihat Alçiçek [a]

[a] Pamukkale University, Department of Geological Engineering, TR-20070 Denizli, Turkey
[b] Hungarian Academy of Sciences, Research Centre for Astronomy and Earth Sciences, Institute for Geological and Geochemical Research, H-1112 Budapest, Budaörsi 45, Hungary
[c] High-precision Mass Spectrometry and Environment Change Laboratory (HISPEC), Department of Geosciences, National Taiwan University, Taipei 10617, Taiwan, ROC
[d] Department of Earth and Atmospheric Sciences, University of Alberta, Edmonton AB T6G 2E3, Canada

ARTICLE INFO

ABSTRACT

In the Denizli Basin (Turkey), located in the western Anatolian extensional province, travertine and tufa deposition has been an ongoing process for at least 600,000 years. Travertine bodies, which are 30 to 75 m thick and each covers areas of 1 to 34 km^2, are up to 1 km^3 in volume.

Today, spring waters in this area have temperatures of 19 to 57 °C, are of the Ca–Mg–HCO$_3$–SO$_4$ type in the Pamukkale, Kelkaya and Pınarbaşı areas and the Ca–Mg–SO$_4$–HCO$_3$ type at Çukurbağ. Thermal waters along the northern margin of the basin are generally hotter than those in the east–southeast and south. The δ^{18}O and δD values of the spring waters indicate a meteoric origin. The average temperatures of the hydrothermal systems in the Denizli Basin appear to have decreased from Pleistocene to Holocene.

Travertine, which formed from the hotter water, is more widespread than the tufa that formed in the cooler spring waters. Deposition of the travertine, which formed largely on slopes, in depressions, and along fissure ridges (mostly on northern basin margins), was controlled by the interplay between various intrinsic and extrinsic parameters. The travertines are formed largely of calcite with only minor amounts of aragonite in some of the vertically banded, crystalline crust, raft and pisoid travertines found in some of the northern sites. The aragonitic samples, rich in Sr, are typically found around the spring orifices and along the central axis of the fissure ridges.

The stable isotope values of the travertine found in the northwest and southeast parts of the basin are different. The δ^{13}C values of the northern travertine deposits are more positive (3.7 to 11.7‰ VPBD) than those found in the south–southeast areas (−4 to 5.8‰ VPDB). In contrast, the travertine and tufa in the southeastern areas have higher δ^{18}O values (−15.2 to −7.8‰ VPDB) than those of the northern areas (−16.6 to −4.8‰ VPDB). Available evidence indicates that spring activity and associated travertine precipitation in the Denizli Basin were controlled largely by tectonic activity rather than by climatic conditions.

1. Introduction

Tufa and travertine that form from spring waters are found throughout the world in many different depositional, climatic, and tectonic settings (Chafetz and Folk, 1984; Ford and Pedley, 1996; Hancock et al., 1999; Arenas et al., 2000; Andrews, 2006). Importance has been attached to these deposits because their depositional, geochemical, and isotopic signatures can provide critical records of past palaeoenvironmental, palaeoclimatic, and tectonic conditions (Chafetz and Folk, 1984; Altunel and Hancock, 1993a; Guo and Riding, 1998; Minissale et al., 2002; Andrews, 2006; Jones and Renaut, 2010). Although open to debate, tufa is herein considered as a deposit that typically contains remains of microphytes, macrophytes, invertebrates, and bacteria (Ford and Pedley, 1996). As such, it corresponds to 'meteogene travertine' as defined by Pentecost (2005). Although tufa generally has low carbon-isotopic values that range from −12 to −4‰ PDB (Arenas-Abad et al., 2010; Özkul et al., 2010), some higher values have been reported (Andrews et al., 1997; Horvatinčić et al., 2005). By comparison, travertine is treated as a hydrothermal deposit that is hard, crystalline, and less porous than tufa (Ford and Pedley, 1996; Pedley, 2009) and generally has more positive δ^{13}C values in the range of −1 to +10‰ (Pentecost, 2005).

Many studies on travertine have been based on a single locality (e.g., Fouke et al., 2000; Kele et al., 2008, 2011) and little attempt has been made to integrate data from numerous springs into one model. Notable exceptions to this general assessment include the studies by Chafetz and Lawrence (1994), Minissale et al. (2002),

and Sant'Anna et al. (2004). Chafetz and Lawrence (1994), for example, integrated information from six calcareous spring systems in U.S.A. and Italy to determine the relationships between the stable isotopic composition of the calcareous spring deposits (i.e., travertine and tufa) and waters from which they were deposited. Similarly, Minissale et al. (2002) demonstrated that there were consistent differences in the geochemical and isotopic signatures of modern and late Quaternary travertines, thermal spring waters, and gas vents on the east and west sides of the Tiber Valley in central Italy.

Travertine deposits are commonly associated with normal or transtensional faults (e.g., Hancock et al., 1999; Brogi and Capezzuoli, 2009). The depositional architecture and geochemical characteristics of travertine deposits are controlled by the balance between extrinsic factors (e.g., climate, spring water composition) and intrinsic factors (e.g., spring flow patterns, biota). Separation of the extrinsic and intrinsic factors can be achieved by comparing different spring deposits found

in one basin. The Denizli extensional basin in western Anatolia, Turkey (Fig. 1A) is ideal for this purpose because it contains numerous carbonate spring deposits (mostly travertine), particularly along its northern boundary (Altunel and Hancock, 1993a; Çakır, 1999; Özkul et al., 2002; Uysal et al., 2009; Özkul et al., 2010; Kele et al., 2011). Accordingly, this paper describes and compares the depositional, mineralogical, and geochemical features of six travertine deposits found in the Denizli Basin with the view of establishing the intrinsic and extrinsic factors that controlled their development. Conclusions reached from these comparisons can provide the basis for evaluating similar deposits throughout the world.

2. Geological setting

The Denizli Basin, located in the Western Anatolian Extensional Province of Turkey (Fig. 1A), is a graben that is bounded by normal
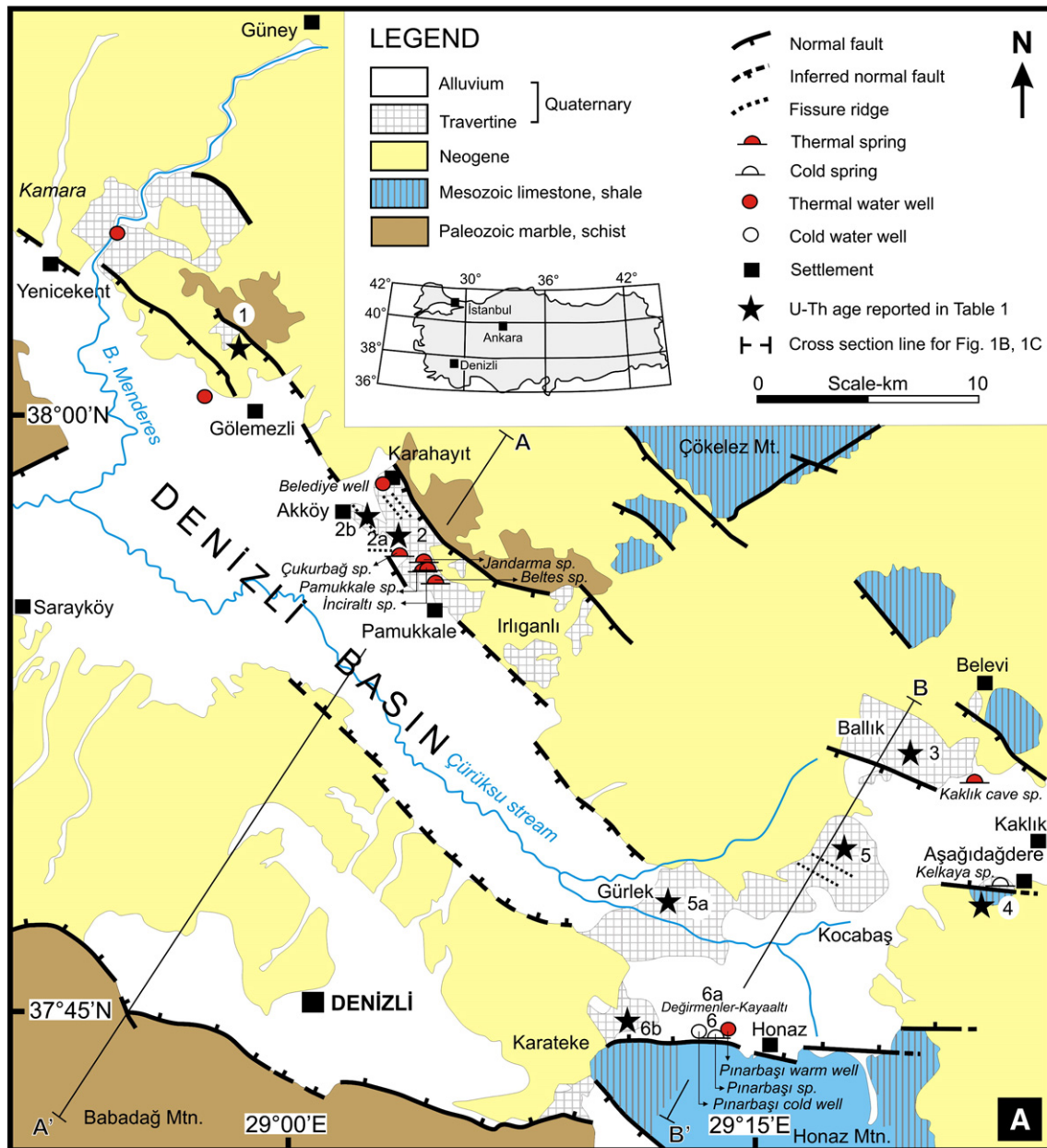

Fig. 1. (A) Geological map showing locations of travertine sites in the Denizli extensional basin (based on Sun, 1990 and Özkul et al., 2002) that was examined in this study. Travertine sites on the map were numbered as: (1) Gölemezli, (2) Pamukkale, (2a) Çukurbağ, (2b) Akköy, (3) Ballık, (4) Kelkaya, (5) Kocabaş, (5a) Gürlek, (6) Honaz, (6a) Değirmenler-Kayaaltı and (6b) Karateke. Locations of the U–Th dated travertines are indicated with stars (see Table 1). A–A′ and B–B′ indicate locations of cross-sections shown in B and C. (B–C) Schematic cross sections along A–A′ and B–B′, respectively (see A).
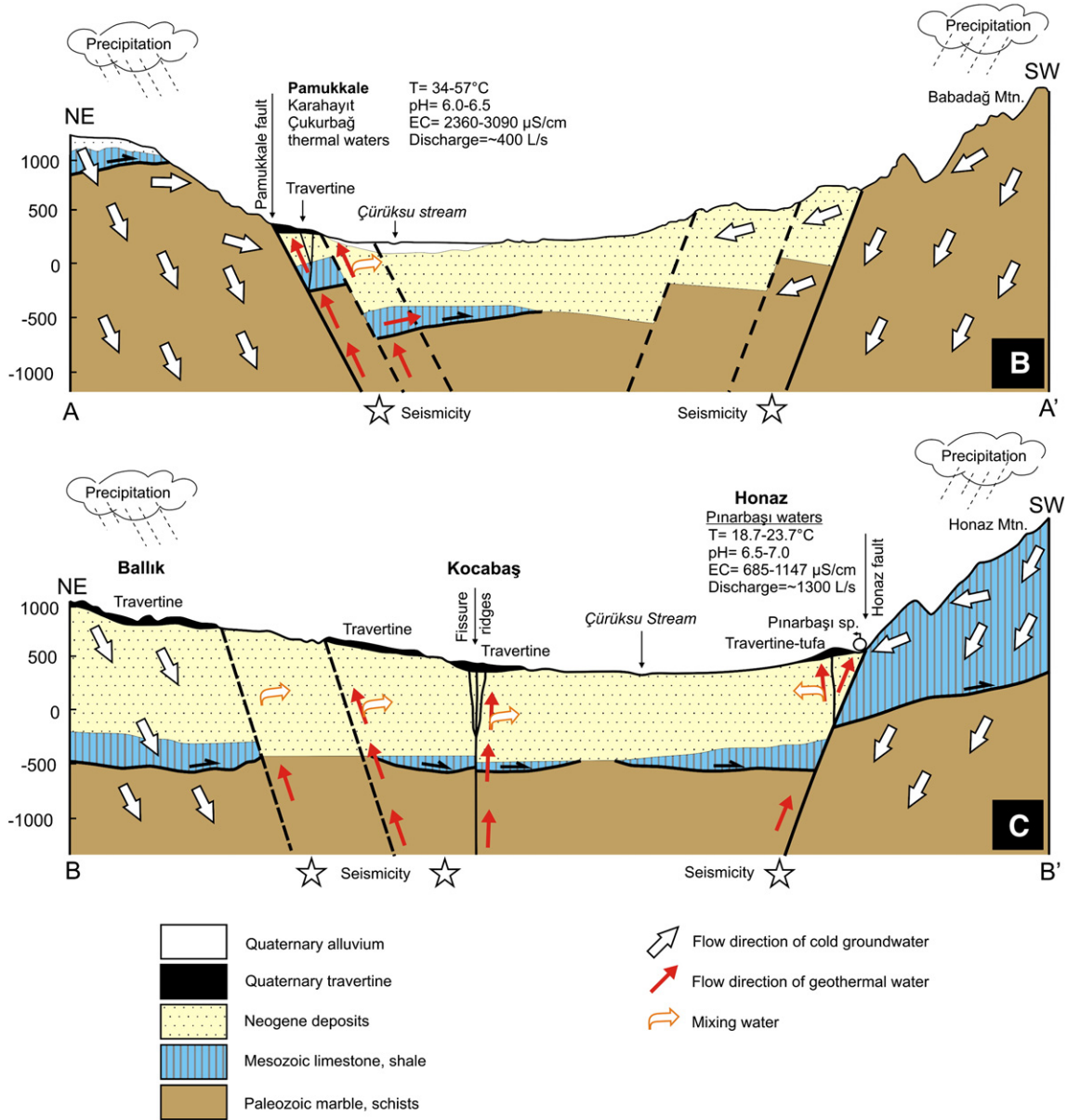
Fig. 1 (*continued*).

faults along its northern and southern margins (Koçyiğit, 2005; Westaway et al., 2005; Kaymakçı, 2006; Alçiçek et al., 2007). The basin includes the Pamukkale travertines and fossil counterparts (Altunel and Hancock, 1993a; Şimşek et al., 2000; Özkul et al., 2002; Kele et al., 2011). Travertine bodies located along the northern margin (Fig. 1A) were deposited at the ends of normal fault segments (e.g., step-over zones; Çakır, 1999).

The Neogene basin fill and old bedrock that underlie the travertine deposits are exposed on the graben shoulders and in the mountainous horst areas (Fig. 1). The bedrock in the main catchment areas, exposed on Honaz (2571 m asl) and Babadağ (2308 m asl) in the south and Çökelez (1840 m asl) in the north, is composed of schists and marbles that cover the Menderes Massif (Bozkurt and Oberhänsli, 2001; Erdoğan and Güngör, 2004) and the allochthonous Mesozoic limestone, dolomite, and gypsum of the Lycian Nappes, which tectonically overlie the Menderes Massif (Okay, 1989).

The Neogene fill in the Denizli Basin is formed from alluvial, fluvial and lacustrine deposits. The basin was initiated as a half graben in the late Early Miocene when deposition gradually evolved from alluvial fan settings into fluvial deposits and finally into lacustrine environments

(Alçiçek et al., 2007). Deposition continued until the Late Pliocene. By the early Quaternary, there was a change in the regional tectonics and the Neogene Denizli half graben became a full graben as the Pamukkale Fault on the north margin became active (Fig. 1B, C). Quaternary deposits are evident on local fluvial terraces that become progressively younger towards the basin centre, and in the form of large travertine deposits that are widespread along the northern and southern margins of the graben. The Quaternary faults and fissures that are common in carbonate bedrock along the margins of the graben are natural pathways that allow meteoric waters to descend into the subsurface and hydrothermal fluids to come to the surface (Minissale et al., 2002; Dilsiz, 2006). These faults and associated fissures cut through the travertine bodies in some localities (Altunel and Hancock, 1993a,b; Van Noten et al., 2013).

The Denizli Basin is important in terms of its seismic activity as well as its geothermal potential (Aydan et al., 2005; Tan et al., 2008; Utku, 2009). The ancient city of Hierapolis at Pamukkale, for example, was damaged several times by earthquakes (Altunel and Barka, 1996; Piccardi, 2007) with magnitudes up to 6.0 (Hancock et al., 2000) that were triggered by normal faulting and extension of the basin (Kaypak

and Gökkaya, 2012). Most of these earthquakes had focal depths of 5 to 15 km. Local seismicity of the Denizli Basin strongly depends on the deep and shallow geothermal systems in the region (Kaypak and Gökkaya, 2012).

3. Sampling and analytical procedures

The travertine exposed at Gölemezli, Pamukkale-Karahayıt (including Çukurbağ and Akköy), Ballık, Kelkaya, Kocabaş and Honaz in the Denizli Basin was examined and sampled between 2006 and 2009. These sites are located in different parts of the basin. The quarry faces provided excellent opportunities for establishing the three dimensional depositional architectures of the deposits. Approximately 65 travertine samples were collected from these sites for mineralogical, petrographical, and geochemical analyses (including stable isotopes), and radiometric dating.

In situ measurements of temperature (T), pH, Eh, and electric conductivity (EC) were carried out using a Hach-Lange HQ40d instrument. The free CO_2 and alkalinity analyses were performed in the field using titrimetric methods. The ions (SO_4, Cl, Ca, Mg, Na, K) and SiO_2 were analyzed with ion chromatography (Dionex ICS-100) and spectrophotometric (Hach DR4000 UV/Vis) methods, respectively. Sr analyses were performed with Optima 2100 DV ICP-OES instrument at the Water Chemistry Laboratory at Pamukkale University, Denizli. Water samples were collected in 100 ml glass bottles for stable isotope analyses of $\delta^{18}O$ and δD. Stable isotope compositions of the waters were determined at the Institute for Geochemical Research of the Hungarian Academy of Sciences (Budapest).

The travertine samples were examined by optical microscope using polished thin sections. Thirteen fracture samples, selected from different sites and various lithotypes, were mounted on stubs and sputter coated with a thin layer of gold before being examined on a JEOL JSM 6490 LV scanning electron microscope (SEM) at the Turkish Petroleum Corporation (TPAO) in Ankara, Turkey. The mineralogical composition of 48 samples was determined by the X-ray powder diffraction (XRD) technique using a Philips PW 1730 diffractometer located at the Institute for Geological and Geochemical Research (Budapest, Hungary) with CuK_α radiation at 45 kV and 35 mA. For this purpose, randomly oriented powders obtained from fresh unweathered samples were used, and semi-quantitative mineral composition was determined according

to the modified method of Bárdossy et al. (1980). For some samples, layers formed from different materials were analyzed separately. If a sample was too small for normal preparation, it was attached directly to a steel slide for analysis. Estimates of the amount of aragonite and calcite in each sample produced by these analyses have a 5–10% error margin.

Cathodoluminescence examination was performed at the Institute for Geological and Geochemical Research, Hungarian Academy of Sciences (Budapest, Hungary) using a Reliotron type cold-cathode equipment that is attached to a Nikon Eclipse E600 optical microscope. The equipment was operated at 8 to 10 kV accelerating voltage with a 0.5 to 1.0 mA current. Photographs were taken with a Nikon Coolpix 4500 digital camera using automatic exposure and a defocused electron beam.

Elemental determinations were completed for 56 samples of recent (i.e., actively forming) and old travertines that came from different sites in the Denizli Basin. These analyses, done by the Acme Analytical Laboratory (AcmeLabs, Vancouver, Canada), utilized inductively coupled plasma mass spectrometer (ICP-MS) techniques. The total abundances of the major oxides and several minor elements are reported on a 0.1 g sample analyzed by ICP-emission spectrometry following a lithium metaborate/tetraborate fusion and diluted nitric digestion. Loss on ignition (LOI) is by weigh difference after ignition at 1000 °C. The TOT/C and TOT/S were determined by Leco. The determination of element composition was performed also by ICP-MS technique, following a lithium metaborate/tetraborate fusion and diluted nitric digestion.

Stable carbon and oxygen isotope values were obtained from 65 samples at the Institute for Geological and Geochemical Research, Hungarian Academy of Sciences, Budapest, Hungary. Carbon and oxygen isotope analyses of bulk carbonate samples were carried out using the conventional phosphoric acid method (H_3PO_4 digestion method at 25 °C) of McCrea (1950) and the continuous flow technique of Spötl and Vennemann (2003). Standardization was conducted using laboratory calcite standards calibrated against the NBS-18, NBS-19 standards. All samples were measured at least in duplicate and the mean values are given in the standard delta notation in parts per thousand (‰) relative to VPDB ($\delta^{13}C$) and VSMOW ($\delta^{18}O$) according to $\delta[‰] = (R_{sample} / R_{reference} - 1) \times 1000$. Reproducibility is better than $\pm 0.1‰$.

Table 1
Uranium and thorium isotopic compositions and ^{230}Th ages for selected travertine samples from locations in the Denizli extensional basin by MC-ICP-MS, Thermo Neptune, at NTU. GL: Gölemezli, ÇB: Çukurbağ, AK: Akköy, KB: Kocabas, GR: Gürlek, OT: Obruktepe (Karateke), KT: Karateke.

Sample no	Weight (g)	^{238}U (ppb)	^{232}Th (ppt)	δ^{234}U measured[a]	$[^{230}\text{Th}/^{238}\text{U}]$ activity[c]	$[^{230}\text{Th}/^{232}\text{Th}]$ (ppm[d])	Age uncorrected	Age corrected[c,e]	δ^{234}U$_{initial}$ corrected[b]
GL-13	0.08970	426.4 ± 1.5	2698 ± 15	43.9 ± 4.3	1.0138 ± 0.0056	2645 ± 19	344,640 ± 18,049	344,490 ± 18,024	116 ± 13
GL14	0.05530	457.14 ± 0.53	44.034 ± 327	70.7 ± 2.0	1.097 ± 0.012	188.0 ± 2.4	613,067 ± ∞	611,230 ± ∞	398 ± ∞
CB-12	0.05530	85.31 ± 0.24	126 ± 13	435.4 ± 5.6	0.3005 ± 0.0030	3350 ± 335	25,348 ± 308	25,321 ± 308	467.7 ± 6.0
AK-34	0.05660	93.07 ± 0.19	1259 ± 13	206.3 ± 4.3	0.1887 ± 0.0025	230.2 ± 3.8	18,483 ± 279	18,188 ± 314	217.2 ± 4.5
KB-20	0.08280	9.209 ± 0.071	3.3 ± 8.4	239 ± 14	0.714 ± 0.011	33,036 ± 84,544	90,471 ± 2645	90,463 ± 2645	308 ± 18
KB-21	0.11304	10.560 ± 0.082	96.9 ± 6.2	152 ± 13	0.6821 ± 0.0083	1228 ± 79	95,301 ± 2607	95,098 ± 2602	199 ± 17
KB-22	0.08418	15.53 ± 0.16	666.1 ± 9.1	180 ± 18	0.894 ± 0.011	344.0 ± 5.4	145,804 ± 6339	144,908 ± 6287	271 ± 28
GRL-1	0.05339	84.17 ± 0.60	124,905 ± 1401	246 ± 10	1.196 ± 0.030	13.31 ± 0.35	261,623 ± 25,496	231,517 ± 26,621	472 ± 42
GRL-2b	0.05040	184.3 ± 1.1	144,009 ± 1783	275.9 ± 8.5	0.921 ± 0.021	19.47 ± 0.49	130,328 ± 5733	114,341 ± 10,011	381 ± 16
GRL-3	0.05720	159.73 ± 0.93	27,375 ± 206	282.3 ± 8.7	0.933 ± 0.011	89.9 ± 1.2	132,047 ± 3481	128,779 ± 3752	406 ± 13
GRL-4b	0.05798	205.7 ± 1.2	3993 ± 101	260.5 ± 9.3	0.8194 ± 0.0061	697 ± 18	109,032 ± 1989	108,652 ± 1988	354 ± 13
OT-1	0.10168	334.9 ± 1.7	66,492 ± 853	123.5 ± 7.3	0.904 ± 0.015	75.1 ± 1.5	168,619 ± 6919	164,143 ± 7014	196 ± 12
OT-2	0.08824	237.2 ± 1.2	21,452 ± 159	114.3 ± 6.4	0.9139 ± 0.0099	166.9 ± 2.0	177,093 ± 5441	175,061 ± 5430	187 ± 11
0T3	0.10113	269.31 ± 0.98	594.0 ± 7.3	76.1 ± 4.5	1.0997 ± 0.0052	8232 ± 104	543,661 ± 111,313	543,618 ± 111,258	354 ± 184
KT-1	0.08908	481.5 ± 1.7	1243 ± 10	74.5 ± 5.8	1.0952 ± 0.0053	7002 ± 59	519,458 ± 110,081	519,406 ± 110,011	324 ± 169

Chemistry was performed on March 20th, 2010 (Shen et al., 2003), and instrumental analysis on MC-ICP-MS (Shen et al., 2012). Analytical errors are 2σ of the mean.
Decay constants are 9.1577×10^{-6} yr^{-1} for ^{230}Th, 2.8263×10^{-6} yr^{-1} for ^{234}U (Cheng et al., 2000), and 1.55125×10^{-10} yr^{-1} for ^{238}U (Jaffey et al., 1971).
[a] $\delta^{234}U = ([^{234}U/^{238}U]_{activity} - 1) \times 1000$.
[b] $\delta^{234}U_{initial}$ corrected was calculated based on ^{230}Th age (T), i.e., $\delta^{234}U_{initial} = \delta^{234}U_{measured} \times e^{\lambda 234 * T}$, and T is corrected age.
[c] $[^{230}Th/^{238}U]_{activity} = 1 - e^{\lambda 230 T} + (\delta^{234}U_{measured} / 1000)[\lambda_{230} / (\lambda_{230} - \lambda_{234})] (1 - e^{-(\lambda 230 - \lambda 234)T})$ where T is the age.
[d] The degree of detrital ^{230}Th contamination is indicated by the $[^{230}Th/^{232}Th]$ atomic ratio instead of the activity ratio.
[e] Age corrections were calculated using an estimated atomic $^{230}Th/^{232}Th$ ratio of 4 ± 2 ppm. The errors are arbitrarily assumed to be 50%.

Travertine samples were gently crushed, ultrasonicated, and dried before U/Th dating. About 50–100 mg for each subsample was selected for U–Th chemistry (Shen et al., 2008) in a class-10,000 geochemical clean room with class-100 benches at the High-Precision Mass Spectrometry and Environment Change Laboratory (HISPEC), Department of Geosciences, National Taiwan University. A triple-spike, ^{229}Th–^{233}U–^{236}U, isotope dilution method (Shen et al., 2003) was employed to correct for instrumental fractionation and determine U/Th isotopic and concentration data (Shen et al., 2002). Measurements of U/Th isotopic abundances were performed on a multi-collector ICP-MS (MC-ICP-MS), Thermo Electron Neptune (Shen et al., 2012). Uncertainties in the U–Th isotopic data were calculated offline (Shen et al., 2002) at the 2σ level and include corrections for blanks, multiplier dark noise, abundance sensitivity, and contents of the four nuclides in spike solution. ^{230}Th dates (before 1950 AD) were calculated using decay constants of 9.1577×10^{-6} yr^{-1} for ^{230}Th and 2.8263×10^{-6} yr^{-1} for ^{234}U (Cheng et al., 2000), and 1.55125×10^{-10} yr^{-1} for ^{238}U (Jaffey et al., 1971).

4. Results

In this section, the travertine sites are described with age determination (Table 1) and the results of water chemistry (Table 2), mineralogical composition (Table 3), and geochemical signatures (Table 4).

4.1. Site descriptions

4.1.1. Gölemezli (site 1)

This fossil site, located ~4 km northwest of Gölemezli village, is found at elevations between 350 and 450 m on a southwest facing hillside (Fig. 1A). The deposit, which is ~35 m thick over an area of <1 km^2, is located at the west end of the NW–SE trending Akköy fault (Çakır, 1999). This fault segment forms the boundary between the Neogene deposits and metamorphic bedrocks. The volume of travertine is estimated to be ~0.035 km^3.

Spaces that developed along the vertical to subvertical fault planes and extensional fissures in the metamorphic bedrocks have been filled by vein travertines that are up to a few metres thick (Fig. 2A). Multiple generations of emplacement are evident from different veins that commonly cross-cut each other (Fig. 2B, C). Downslope, the light green and honey coloured banded travertines pass into the bedded travertines. Vein travertines from this site yield U–Th ages of 344 ± 18 ka, and 613 ka (Table 1).

4.1.2. Pamukkale (site 2)

This huge travertine deposit, ~6.0 km long, is located on the hanging block of the northwest-trending Pamukkale Fault m (Fig. 1A) at elevations between 250 and 400 m (Altunel and Hancock, 1993a,b; Ekmekçi et al., 1995; Şimşek et al., 2000). In this study, Karahayıt is regarded as a subsite of the Pamukkale travertine site because of depositional and geochemical differences in the precipitates and water temperatures (Gökgöz, 1994; Şimşek et al., 2000; Şimşek, 2003).

The Karahayıt subsite, located northwest of Pamukkale (Fig. 1A, B), is characterized by thermal water with a temperature of ~53 °C (Table 2) that emerges from a fissure and precipitates red to brown travertine that is covered with microbial mats (Fig. 3A, B). Consequently, the local people call it 'Kırmızı Su' (meaning red water in Turkish).

The Pamukkale travertine, designated as a UNESCO world heritage site (Şimşek, 2003), is characterized by its dazzling white colour. The ancient Roman city of Hierapolis, built on this site, is at 365 m asl. The warm waters (~35 °C) that flow from four springs which are located along the Pamukkale Fault and connected fissures (Fig. 1A, B), are now directed to the slope aprons by a closed concrete channel system (Gökgöz, 1994; Şimşek et al., 2000; Kele et al., 2011). Precipitation

Table 2
Chemistry of the travertine-depositing waters in the study area.

Group	Site and name	Latitude	Longitude	Elev. (m)	T (°C)	EC (µS/cm)	pH	CO$_2$ (ppm)	Ca	Mg	Na	K	HCO$_3$	SO$_4$	Cl	SiO$_2$	Sr	δ^{18}O (‰ SMOW)	δ^{2}H (‰ SMOW)	Charge balance (%)	log[a] pCO$_2$	S.I.[a] calcite
I	Karahayıt																					
	Belediye well	N37°57'33"	E29°06'32"	338	53.0	2770	6.7	384	449	114	115	23.0	947	961	26.9	61.6	9.09	−8.1	−51.8	2.00	−0.61	0.87
	Çukurbağ spring	N 37°55'88"	E29°07'10"	290	57.1	3090	6.5	548	527	114	128	25.5	1235	980	26.5	44.0	7.62	−8.3	−58.9	0.81	−0.27	0.88
	Pamukkale																					
II	Beltes spring	N37°55'44"	E29°07'57"	360	34.4	2360	6.1	502	446	86	39	5.2	945	660	9.6	47.8	6.37	−9.0	−58.7	3.47	−0.13	0.09
	İnciraltı spring	N37°55'57"	E29°07'58"	366	34.2	2380	6.1	488	450	94	42	5.5	940	677	9.6	50.8	6.49	−8.8	−58.0	4.90	−0.14	0.08
	Özel İdare spring	N37°55'56"	E29°07'56"	360	33.7	2400	6.0	486	452	88	42	5.7	945	682	9.9	48.8	6.09	−8.9	−58.5	3.71	−0.04	−0.02
	Jandarma spring	N37°55'66"	E29°07'48"	360	32.9	2370	6.2	400	462	89	41	5.6	955	682	10.0	46.4	6.07	−8.9	−58.7	4.41	−0.24	0.18
	Kelkaya-Kaklık																					
III	Kelkaya spring	N37°48'60"	E29°23'16"	561	18.7	1932	7.4	82	337	91	11	2.0	556	720	12.1	27.9	4.99	−8.5	−53.2	1.01	−1.76	0.85
	Kaklık cave spring	N37°51'35"	E29°23'14"	528	22.8	1769	6.6	66	285	80	28	3.3	432	705	34.0	32.0	5.15	−8.1	−52.9	−1.75	−1.03	−0.06
	Honaz																					
IV	Pınarbaşı spring	N37°45'25"	E29°14'80"	503	18.7	685	7.0	36	98	30	10	1.0	272	136	4.0	17.3	1.16	−8.8	−55.8	3.03	−1.63	−0.19
	Pınarbaşı cool well	N37°45'27"	E29°14'77"	503	19.8	833	6.9	32	127	34	9	1.5	342	178	4.0	17.5	1.30	−8.9	−56.8	5.48	−1.43	−0.10
	Pınarbaşı warm well	N37°45'26"	E29°14'83"	503	23.7	1147	6.5	96	180	45	17	2.2	468	243	7.0	21.0	1.64	−8.8	−55.8	2.41	−0.88	−0.20

Parkhust, D.L., 1995, User's guide to PHREEQC—A computer programme for speciation, reaction path, advective transport, and inverse geochemical calculations: U.S. Geological Survey Water Resources Investigations Report 95-4227, 143 p.

[a] The saturation index with respect to calcite and partial pressure of CO$_2$ of the waters were computed using PHREEQC (Parkhust, 1995).

Table 3
Mineralogical compositions of the travertine samples collected from different sites in the Denizli Basin based on XRD analyses. Ca: Calcite, Ar: Aragonite, Do: domite, Gy: gypsum, Q: quartz, Mi: Mica, Cl: Clorite, Ka: Kaolinite, KF: K-Feldspar, Gt: goethite Ra: rancieite, Sm: smectite, Il: illite, tr: trace amount.

Site name	Sample no	Travertine type	Ca	Ar	Do	Gy	Q	Mi	Cl	Ka	Sm	Il	Kf	Pl	Gt	Ra
Gölemezli	GL-1	Vertically banded	100				tr									
(1)	GL-2	Vertically banded	100				tr									
	GL-6	Vertically banded	100				tr									
	GL-8	Bedded	100		tr		tr									
	GL-9	Bedded	80		14		5	1	tr				tr			
	GL-10	Raft	95		3		tr	tr	tr				tr	tr		
Pamukkalee	PK-4	Crystalline crust	99			tr	tr									
(2a)	PK-5	Crystalline crust	100													
	PK-5b	Ooid	100				tr									
	PK-6	Crystalline crust	100													
	PK-7	Crystalline crust	100													
	PK-7b	Pisoid	100													
	PK-8	Pisoid	99				tr	tr								
	PK-9	Crystalline crust	95				3	1								
	PK-10	Crystalline crust	100													
	PK-11	Crystalline crust	100													
	PK-12	Crystalline crust	100				tr									
	PK-13	Crystalline crust	99				1									
Çukurbağ	ÇB-6	Crystalline crust		100												
(2b)	ÇB-7	Raft	95	5												
	ÇB-9	Ooid	22	78												
	ÇB-10	Crystalline crust	100				tr									
	ÇB-11a	Vertically banded	77–100	7–23												
	ÇB-12 brown	Vertically banded	99				tr								1	
	CB-12 white	Vertically banded	30	70												
Akköy	AK-8	Bedded	99				tr								tr	
(2c)	AK-10	Bedded	98												2	
	AK-12	Raft and micrit	100													
	AK-15	Bedded	94				4	1				1				
	AK-45	Bedded	100				tr									
Ballık	BA-2	Bedded	90													10
(3)	BA-3	Bedded	65				15		3	4	3				10	
	BA-4	Bedded	95				4			<1	<1	tr	tr			
	BA-5	Bedded	100				tr									
	BA-6	Bedded	100				tr									
	BA-7	Bedded	100				tr									
	BA-8	Bedded	100				tr									
Kelkaya	KL-1	Bedded	100													
(4)	KL-2	Bedded	100													
	KL-3	Bedded	100													
Kocabaş	KB-1	Vertically banded	25	75												
(5)	KB-2	Vertically banded	93	7												
	KB-6	Bedded	100				tr									
	KB-11	Bedded	98				2									
Honaz	KT-22	Oncolith	100													
(6)	KT-23	Tufa	100				tr									
	KT-24	Tufa	100				tr									

from these spring waters (Table 2) has produced the vast white calcite deposits with their spectacular arrays of terraces and rimstone pools (Ekmekçi et al., 1995) (Fig. 3C, D). The white slopes are covered mostly by crystalline calcite, whereas lime mud (Fig. 3E), shrubs, pisoids, rafts, and coated gas bubbles are common in the terrace pools (Özkul et al., 2002; Jones and Renaut, 2008; Kele et al., 2011).

The first U–Th ages from the fossil travertine at Pamukkale, obtained by Altunel (1994, 1996), ranged from 24 to 400 ka. More recently, a U–Th age of 55.4 ka was obtained from the vertically banded travertines along the scarp of the Pamukkale fault (Uysal et al., 2007).

The Çukurbağ subsite is located near the slope apron, just in front of Jandarma spring, Pamukkale, which lies at an altitude between 250 and 300 m asl, and encompasses a relatively flat to gently concave area that is characterized by several fissure ridges that are variably oriented. The E–W trending Çukurbağ fissure ridge (Fig. 4A), is ~400 m long, 10 m high, and 40 m wide (Altunel, 1994). Past quarrying has exposed the central part of the ridge (Fig. 4A–C). Samples from the vertical bands that fill the central fissure space (Fig. 4B, C) yielded U-series ages that range from ~24.7 to 152 ka (Uysal et al., 2007, 2009). One sample from the banded travertines (Fig. 4B, C), collected during this study, yielded a U–Th age of 25.3 ka (Table 1).

Today, a mesothermal spring with a temperature of 57.1 °C (Table 2) is located at the east end of the Çukurbağ ridge. Travertine is presently being precipitated in small, shallow pools (a few metres wide) and narrow channels that are located around the spring orifice. Calcite rafts and coated gas bubbles around the pool margins are associated with thermophilic microbial mats (Fig. 4D, E).

The Akköy subarea, situated ~1 km southeast of Akköy town at ~250 m asl and southwest of the Karahayıt-Pamukkale travertine plateau, is dominated by a large fissure ridge (Figs. 1, 5A). The northwest trending ridge, 1400 m long, 40 m high, and up to 800 m wide at its base, is also known as 'Karakaya Hill' or the 'Akköy fissure ridge' (Altunel, 1994). A depression lies between the ridge and the Karahayıt subarea to the north. Recent quarrying provides a three-dimensional view of the structure and depositional architecture of the Akköy ridge (Fig. 5A–C). Secondary fissures are associated with the main fissure (Altunel, 1994). The fissure spaces in the ridges are filled with vertically banded/vein travertines (Fig. 5B), which become younger towards the central part of the fissure space (Altunel et al., 1993a,b). Some veins bifurcate towards the surface and cross cut the older bedded travertines (Uysal et al., 2009). Evidence of repeated fracturing and filling events are apparent in some of the fissures (Fig. 5C, D).

Table 4
Element and stable isotopic compositions of travertine samples from the different sites in the Denizli Basin.

Site no	Sample ID	Travertine type	Ca	Mg	Fe	Mn	Sr	$\delta^{13}C$	$\delta^{18}O$	$\delta^{18}O$
			(ppm)					(‰V-PDB)	(‰V-PDB)	(‰V-SMOW)
Gölemezli	GL-1	Vertically banded	398,214	5040	<280	232	1073	3.8	−16.0	14.5
(1)	GL-2	Vertically banded	397,857	5040	350	387	1156	3.8	−16.6	13.8
	GL-3	Vertically banded	396,571	4560	1679	542	660	4.0	−13.1	17.4
	GL-4	Vertically banded	368,429	6960	2868	155	751	3.7	−15.2	15.2
	GL-5	Vertically banded						−0.3	−15.1	15.4
	GL-6	Vertically banded	392,214	8160	629	155	1756	3.7	−15.0	15.5
	GL-7	Vertically banded						4.6	−15.0	15.4
	GL-8	Bedded	405,214	2640	769	77	769	5.0	−13.9	16.6
	GL-9	Bedded	329,857	20,940	4896	155	586	4.8	−13.2	17.3
	GL-10	Raft	340,929	5940	6365	155	484	4.0	−15.4	15.1
Pamukkale	PK-4	Crystalline crust	401,000	3240	560	<77	2991	11.3	−9.3	21.3
(2)	PK-5	Crystalline crust						6.1	−10.7	19.9
	PK-5b	Pisoid	394,429	4080	280	<77	1971	6.6	–	–
	PK-6	Crystalline crust						5.9	−10.2	20.4
	PK-7	Crystalline crust						5.9	−10.6	20.0
	PK-7b	Pisoid	396,643	4440	<280	<77	1973	6.4	–	–
	PK-8	Pisoid	402,571	3240	<280	<77	2219	5.8	−11.1	19.5
	PK-9	Crystalline crust	349,214	3840	2098	<77	1920	7.1	−10.3	20.3
	PK-10	Crystalline crust	400,786	3060	<280	<77	2346	8.2	−10.5	20.1
	PK-11	Crystalline crust						9.7	−9.7	20.9
	PK-12	Crystalline crust	396,214	3840	<280	<77	3028	11.5	−9.0	21.6
	PK-13	Crystalline crust	398,643	3720	839	<77	2715	11.7	−9.1	21.5
Çukurbağ	ÇB-6	Crystalline crust	396,429	120	<280	<77	7392	4.3	−15.6	14.8
(2a)	ÇB-7	Crystalline crust	392,000	4320	2308	77	3771	5.8	−14.0	16.5
	ÇB-8	Raft and coated gas bubble	393,214	5760	1678	77	3113	5.5	−13.3	17.2
	ÇB-9	Ooid	390,571	2940	2378	77	2306	4.3	−15.2	15.2
	ÇB-10	Crystalline crust	398,500	2280	<280	1162	1285	4.7	−4.8	26.0
	ÇB-11	Banded	396,714	180			6822	5.2	−15.8	14.6
	ÇB-12a	Banded	396,000	780	2238		5692	5.3	−16.6	13.8
	ÇB-13	Banded	398,214	1740	560	77	2215	5.1	−11.1	19.5
Akköy	AK-1	Raft	401,571	4980	2308	155	1540	5.6	−12.4	18.1
(2b)	AK-3	Bedded	392,214	1980	7204	155	803	5.3	−10.6	20.0
	AK-4	Bedded	389,500	960	16,157	542	410	5.6	−9.1	21.5
	AK-5	Raft	386,500	1740	16,786	310	549	5.9	−9.2	21.4
	AK-6	Bedded	332,286	6120	13,009	232	1677	4.3	−10.9	19.6
	AK-8	Bedded	367,000	1860	37,209	232	705	8.0	−10.3	20.3
	AK-10	Bedded	388,929	1920	7414	542	615	6.2	−10.8	19.8
	AK-11	Bedded	380,786	1920	10,911	232	660	7.0	−9.7	20.9
	AK-12	Raft	391,714	2280	6085	232	548	7.3	−10.8	19.7
	AK-15	Bedded	391,286	1860	3007	77	564	7.8	−8.6	22.1
Ballık	BA-1	Crystalline crust	382,714	1560	<280	<77	1590	−1.7	−8.7	22.0
(3)	BA-2	Dark coloured, manganiferous	276,286	3960	2238	27,648	190	−0.4	−8.9	21.8
	BA-3	Bedded, reddish brown	350,071	4920	75,325	1471	250	−3.3	−8.5	22.1
	BA-4	Bedded	401,857	1500	6225	774	796	0.6	−7.8	22.8
	BA-5	Bedded	384,785	2760	769	154	184	−0.1	−8.8	21.8
	BA-6	Bedded	395,000	3240	3497	<77	274	−0.6	−11.1	19.5
	BA-7	Bedded	394,214	3540	<280	77	398	0.3	−11.4	19.2
	BA-8	Bedded	396,643	3240	<280	<77	457	−0.2	−9.6	21.0
	BA-9	Bedded	396,643	3240	<280	<77	458	−0.2	−9.6	21.0
	BA-10	Bedded	397,929	2640	<280	<77	329	0.8	−8.7	21.9
	BA-11	Bedded	396,000	2280	490	<77	296	−0.1	−9.8	20.9
Kelkaya	KL-1	Bedded	355,274	6091	<280	<77	2103	3.4	−8.2	22.4
(4)	KL-2	Bedded	361,420	3316	<280	<77	2181	5.8	−8.1	22.6
	KL-3	Bedded	361,849	3558	2098	<77	2330	3.2	−8.9	21.7
Kocabaş	KB-1	Vertically banded						5.6	−13.5	17.0
(5)	KB-2	Vertically banded						4.4	−15.2	15.3
	KB-3	Vertically banded						4.7	−13.7	16.8
	KB-4	Vertically banded						4.7	−14.3	16.2
Honaz	HO-1	Tufa, Karateke	387,221	5669	1748	<77	856	−4.0	−10.3	20.3
(6)	HO-2	Tufa, Karateke	397,798	3437	699	<77	439	2.6	−9.6	21.0
	HO-3	Tufa, Karateke	397,071	3360	<280	<77	462	2.9	−9.7	20.9
	HO-4	Bedded tr., Obruktepe	398,643	2400	<280	<77	644	4.7	−9.4	21.2
	HO-5	Tufa, Değirmenler	379,928	4080	699	<77	975	−0.9	−9.4	21.2
	HO-6[a]	Tufa, Değirmenler	379,214	7380	769	<77	1053	−0.4	−9.2	21.4
	HO-7[a]	Tufa, Kayaaltı	–	–	–	–	–	1.8	−10.0	20.5
	HO-8[a]	Tufa, Kayaaltı	373,214	4140	1608	<77	844	0.1	−8.3	22.3

[a] From Horvatinčić et al. (2005).

Bundles of raft flakes, earlier considered as bedded travertine (Uysal et al., 2009, their Fig. 2E), red mudstones rich in Fe-oxide, and angular clasts of older travertine and metamorphic bedrocks are found in some of the fissures (Fig. 5C–E). The white, horizontal ledges (Fig. 5E) formed when the fissure spaces were filled with thermal waters. Some rafts were thickened due to subsequent encrustation (cf., Guo and Riding, 1998) whereas other rafts are now in vertical to subvertical positions.
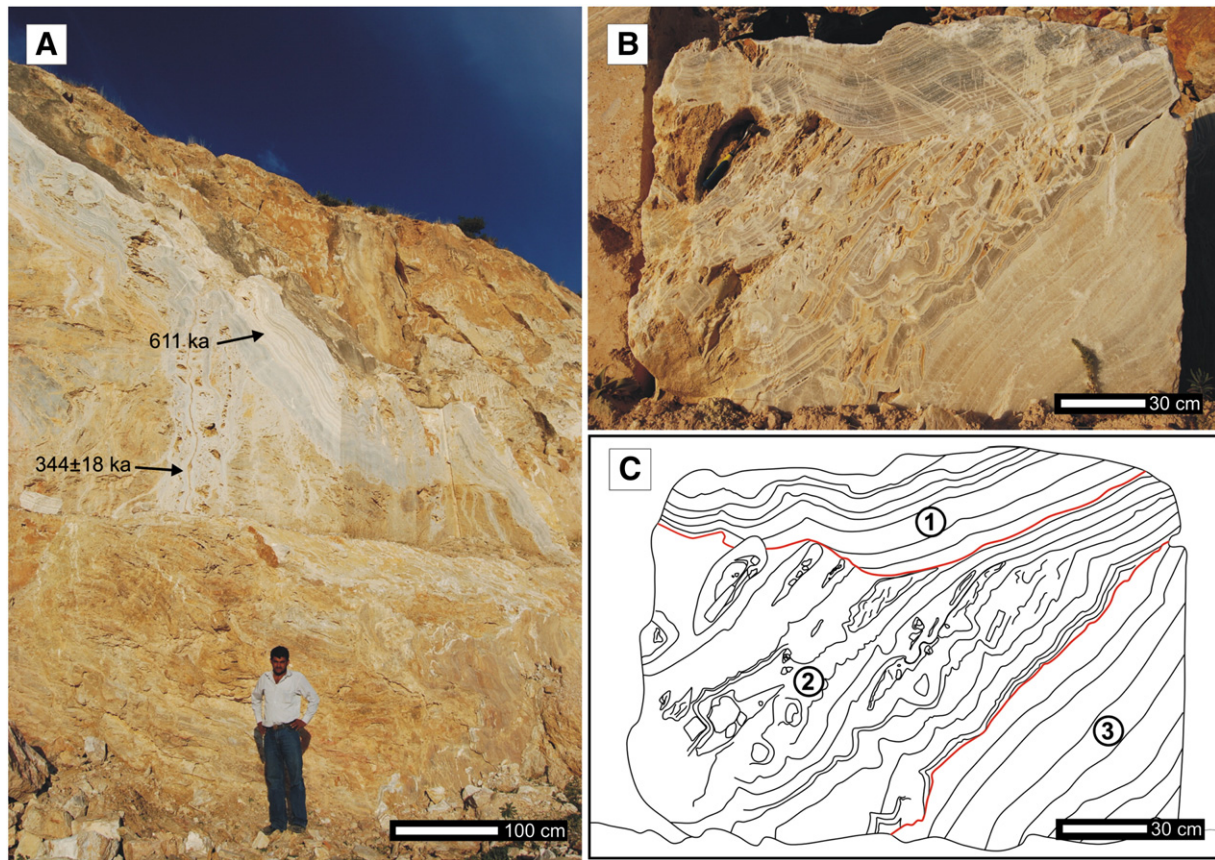
Fig. 2. Field views of Gölemezli travertine site. (A) Vein travertines with network appearance located along steeply dipping fault planes and fractures in metamorphic bedrock, exposed in quarry wall. U–Th dates are shown. View to northeast. (B) Cut surface showing cross cutting relationships between different generations of vein travertine. (C) Interpretation of surface shown in panel B, indicating vein generations 1, 2 and 3.

Bedded travertine, which dips at 10–20° away from the ridge crest, is present on both sides of the fissure axis (Fig. 5A, B). These beds are formed from alternating layers of crystalline shrubs, rafts, micrite, and coated gas bubbles (Fig. 5F–H). Palaeosols, up to 60 cm thick, and lithoclast interbeds are found in some parts of the succession. A sample from the uppermost part of the fissure ridge gave a U–Th age of 18.4 ± 0.3 ka (Table 2).

The Pamukkale travertine plateau, which includes the Karahayıt, Çukurbağ and Akköy subsites, has an average thickness of 50 m and covers an area of 11.8 km². Thus, the volume of travertine is estimated to be about 0.6 km³.

4.1.3. Ballık (site 3)

Ballık, located ~5 km northwest of Kaklık, has travertine deposits that are exposed on a stepped southwest facing slope (Fig. 1A, C) that is 500 to 1000 m asl. It is the largest travertine site in the basin with travertine up to 120 m (average 75 m) thick that covers an area of 12.5 km². The volume of travertine at this site is approximately 0.94 km³. The travertine deposit is dissected by northwest-trended normal faults and extensional fractures.

Today, there are about 50 quarries operating in this area. The cut surfaces in the quarries allow investigation of the spatial architecture of the depositional settings that developed as the travertines were being deposited. In the Ballık area, the travertine sequences are formed mostly of horizontally to subhorizontally bedded travertine, particularly in the lower and middle parts (Fig. 6A, B), that extends laterally for a few hundred metres. These successions are formed mainly of thin shrub layers, micritic laminae, coated bubbles, and locally included reed casts. Throughout the successions exposed in the quarries there are intercalations of fluvial conglomerate, sandstone,

and red and green mudstone (Fig. 6A, B), palaeosol horizons, and erosional surfaces (Özkul et al., 2002). At Killik Tepe, south of this area, the horizontally bedded travertines at the base pass gradually upward into the low angle slope travertine that, in turn, passes upward into the tufa facies at the top (Fig. 6C, D). The slope facies is composed mainly of crystalline calcite, shrub, and micritic layers that are locally cut by erosional surfaces.

The uppermost tufa horizon, which can be followed laterally for several hundred metres, is formed from numerous mound and waterfall build-ups, each of them are convex upward and dominated by reed and bryophyte tufa. The mound facies, up to 25 m thick, typically have high porosity due to the presence of big cavities of a few metres in diameter and reed cast moulds (Fig. 6C, D).

4.1.4. Kelkaya (site 4)

This travertine at this site, located near the village of Aşağıdağdere, is at the foot of the north facing slope of the Kelkaya Hill at elevations between 520 and 750 m asl (Fig. 1A). Kelkaya Hill is formed from Mesozoic limestone bedrock. The travertine is ~50 m thick and covers an area of 0.75 km². The estimated volume of travertine is 0.04 km³. The spring waters arise along a normal fault plane that dips to the north. Waterfall tufas with porous textures dominate the upper part of the site (Fig. 7A). In contrast, the horizontally bedded and low-angle slope travertines that dip to the north cover the lower part of the area (Fig. 7A). The terrace pools and their rims are clearly evident on the vertical wire-cut surfaces (Fig. 7B). In the quarry, the uppermost bench (~10 m high) is separated from the lower benches by a palaeosol and green claystone horizons.
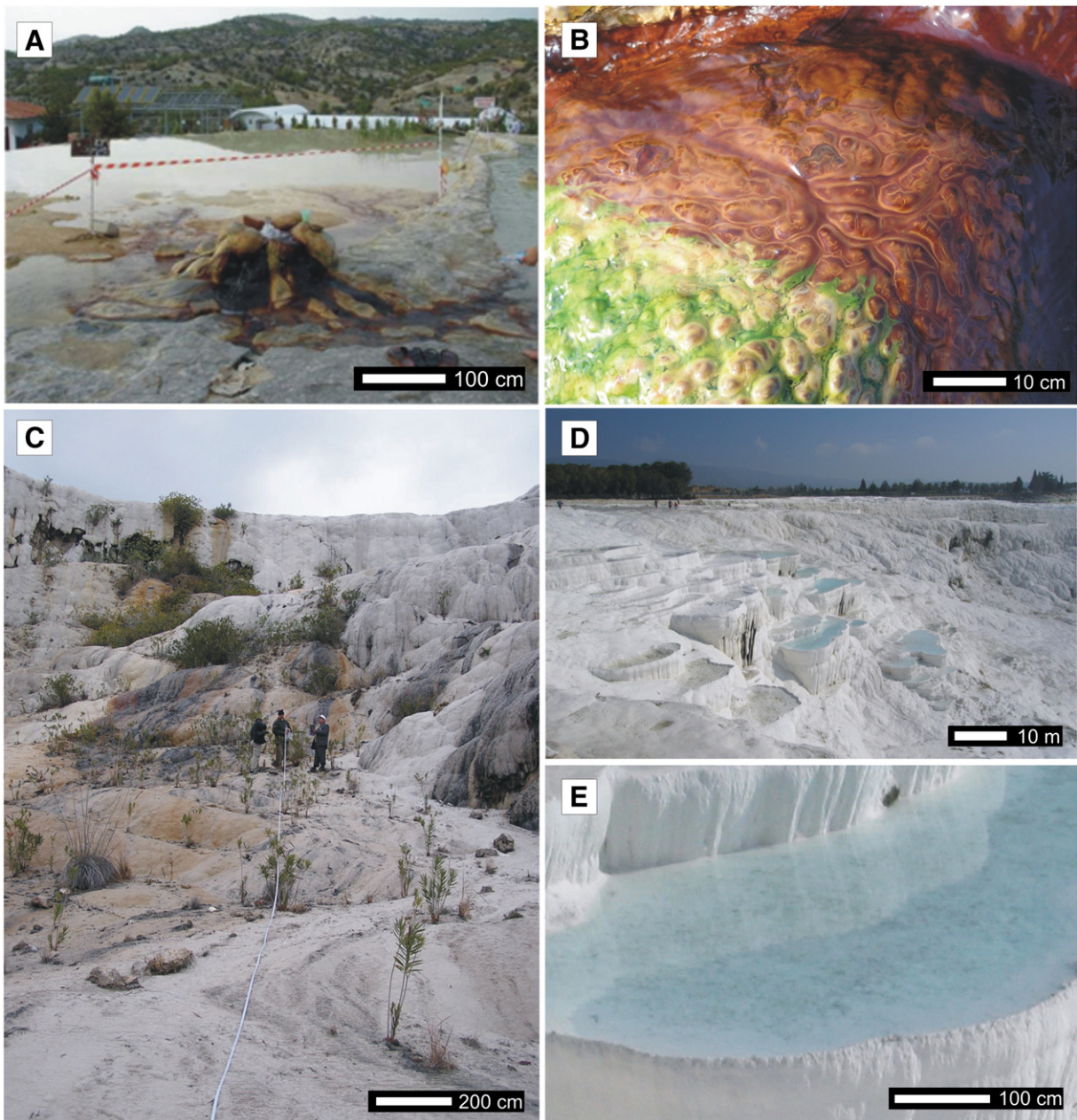
Fig. 3. Field photographs from Karahayıt-Pamukkale. (A) Thermal water, with a temperature of ~53 °C, discharging from a pipe that has been placed in spring vent at Karahayıt. Note reddish coloured travertine and green microbial algal mat on surface. (B) Surface of travertine partly covered by green microbial algal mat. (C) Stepped slope formed from travertine, slope apron in front of the Jandarma spring, Pamukkale. (D) Terraced slope travertines at Pamukkale, terrace pools filled with water. (E) Terrace pool lined by rimstone with lime mud on floor of pool.

4.1.5. Kocabaş (site 5)

Travertines around the villages of Kocabaş and Gürlek, herein referred to as the Kocabaş site (Fig. 1A, C), are located on a relatively flat area that lies between 370 and 495 m asl. In this area, the travertine is ~40 m thick and covers an area of ~33.7 km². The estimated volume of travertine is about 1.0 km³. Highway 320 (from Denizli to Afyon) passes through the site. The area, bounded to the north by the Ballık site, is formed mainly of several NW-trending inactive fissure ridges that are flanked by bedded travertines (Özkul et al., 2002; Altunel and Karacabak, 2005). The main fissures in the ridges are filled by vertically banded travertines that are up to 16 m thick. Based on the observation from the quarry faces that are perpendicular to the main fissure axis, the bedded travertines (Fig. 8A), with thickness up to 50 cm, dip away at angles of 5–10°. Within the bedded travertine, bedding-parallel crystalline layers, up to 60 cm thick

(Fig. 8A, B), are formed almost entirely of calcite and/or aragonite (Table 3). The bedding-parallel crystalline layers (or veins) are commonly brecciated (Fig. 8B, C) and similar to the 'jigsaw puzzle' or 'crackle textures' found in the Akköy fissure ridge near Pamukkale (Uysal et al., 2009). In the Kuşgölü fissure ridge, immediately north of Highway 320, vertical and horizontal veins cut the bedded travertines and each other many times (Fig. 8E, F). U–Th dates obtained from these vertical and horizontal veins yielded ages of 90.5, 95.1, and 144.9 ka (Table 1). Thermoluminescence dates of 330 ± 30 and 390 ± 40 ka (Özkul et al., 2004) and U–Th dates of 105 ± 9.8 to >400 ka (Altunel and Karacabak, 2005; De Filippis et al., 2012) have been obtained from samples collected from this travertine.

Near Gürlek (site 5a), ~7 km west of Kocabaş (Fig. 1A), the horizontally bedded travertines are exposed at ~370 m asl. The travertine benches are composed of light, medium and dark coloured horizons
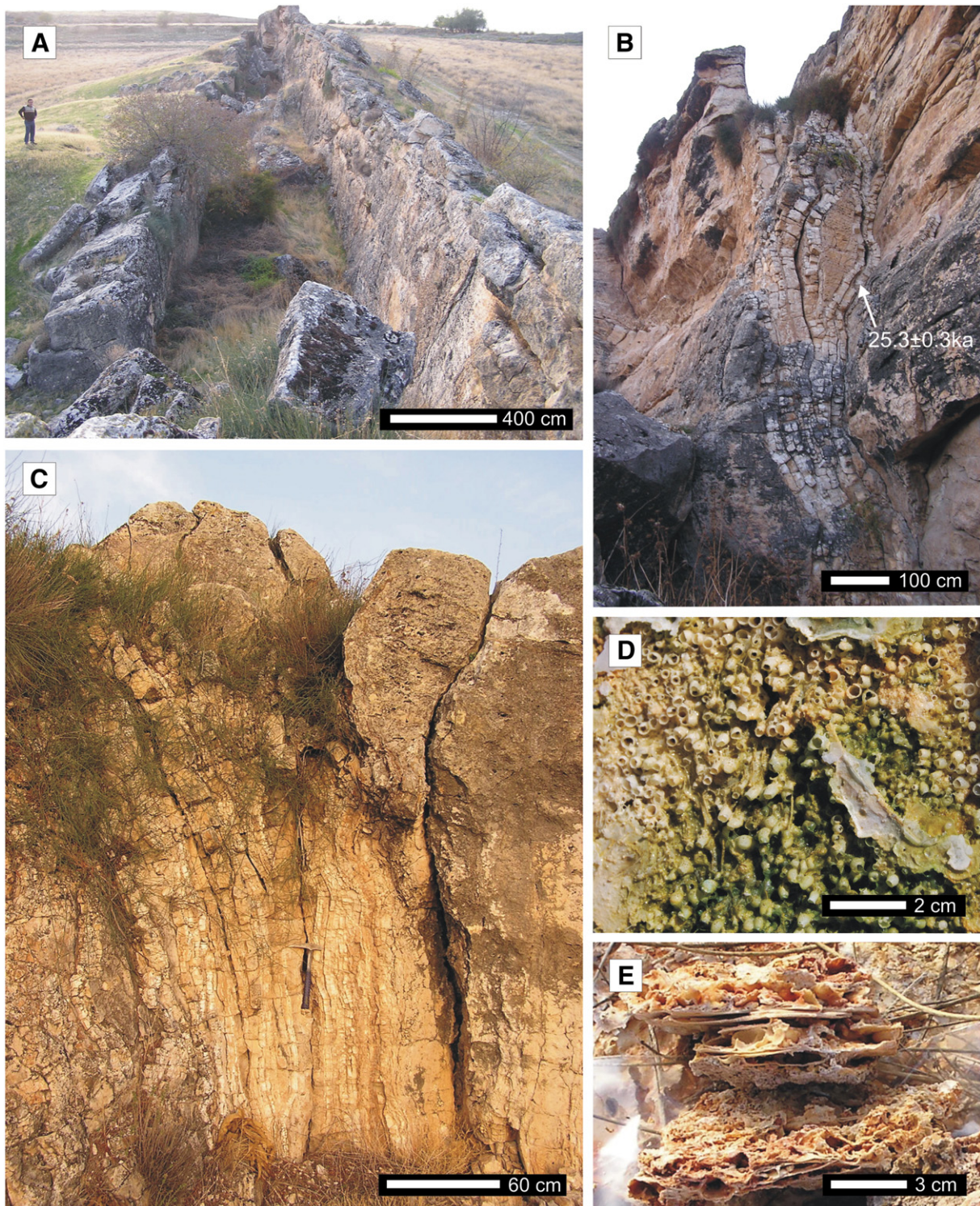
Fig. 4. Field photographs of Çukurbağ. (A) Westward view of the Çukurbağ fissure ridge, partly exposed by quarrying. (B) Vertical banded and associated bedded travertine in central part of ridge with U–Th date. (C) Vertical bands expanding upward, eastern end of the quarry shown in panel A. (D) Recent coated gas bubbles, rafts and microbial mat on the pool surface around Çukurbağ hot spring, eastern end of ridge. (E) Recent to subrecent, rafts and associated coated gas bubbles.

(Fig. 9A) that are locally interbedded with palaeosols, claystone, and mudstones. Some of the medium and dark horizons contain numerous gastropods. Travertine samples from the quarries yielded U–Th ages of 231.5 ka, 128.8 ka, 114.3 ka and 108.7 ka (Table 1).

4.1.6. Honaz (site 6)

This area is (site 6) located at the west end of the east–west trending Honaz Fault, which forms the southern margin of the basin

(Fig. 1A, C) and is still seismically active today (Bozkuş et al., 2000). Sites at Değirmenler, Kayaaltı and Karateke are included in the Honaz site. Both travertine and tufa are found at these localities (Fig. 9A–D). At Honaz, the travertine is 30 m thick and covers an area of 2.7 km². The volume of travertine is estimated at 0.08 km³. At Kayaaltı (subsite 6a), fossil tufa of Holocene age is exposed on a northwest facing cliff face (Fig. 9B) that is ~20 m high (Horvatinčić et al., 2005). The upper part of this tufa body is formed from the

waterfall facies (Fig. 9B), with hanging tufa curtains and primary cavities (cf., Pedley et al., 2003; Özkul et al., 2010). Below the waterfall, the distal slope is covered with subhorizontally bedded detrital tufas. Today, tufa precipitation is restricted to the Değirmenler subsite (Horvatinčić et al., 2005). Older tufa and travertine samples (KT-2, OT-3), collected near Karateke (Fig. 9C), yielded U–Th ages of 519.4 ka and 543.6 ka (Table 1). Two other samples (OT-1, OT-2) from the travertine quarry at the Obruk Tepe nearby Karateke (Fig. 1A) yielded U–Th ages of 164.1 ka and 175.1 ka (Table 1).

4.2. Water chemistry

Today, travertine precipitating spring waters belong to four groups (I to IV) based on their physico-chemical features and locations in the basin: (I) Karahayıt and Çukurbağ, (II) Pamukkale, (III) Kaklık cave and Kelkaya, and (IV) Honaz (Table 2). The reservoir rocks for the thermal waters in the Karahayıt and Çukurbağ sites are Palaeozoic marble, whereas the main aquifers supplying warm and mineralized water to the Pamukkale thermal springs are Palaeozoic marbles and Mesozoic limestones (Şimşek et al., 2000).

Thermal waters from the springs and wells discharge at various temperatures. Relatively higher temperature thermal waters (32.9–57.1 °C) arise along the northern margin of the basin at Karahayıt, Pamukkale and Çukurbağ, whereas the waters with lower temperature (18.7–23.7 °C) appear in and around Kaklık cave and Kelkaya to the southeast and Honaz to the south (Fig. 1A, Table 2).

The pH of waters in the study area varies from 6.0 to 7.4 (Table 2) and increases up to 7.8 towards the distal parts of discharge aprons at Pamukkale (Kele et al., 2011). The electrical conductivity (EC) values of the thermal waters vary between 2770 and 3090 μS/cm in Karahayıt and Çukurbağ, 2360–2400 μS/cm at Pamukkale and 1769–1932 μS/cm at Kelkaya-Kaklık. Honaz waters have lower EC values (685–1147 μS/cm). Electrical conductivity, almost all ions, SiO_2 and Sr values of the waters in the basin increase with increasing water temperature (Table 2). The waters in the springs at Pamukkale and Pınarbaşı and associated wells are of the $Ca–Mg–HCO_3–SO_4$ type. In contrast, the waters from the Çukurbağ thermal spring, well KH-3 in Karahayıt, Kaklık cave and Kelkaya are of the $Ca–Mg–SO_4–HCO_3$ type (Table 2). Basin-wide, the $\delta^{18}O$ and δD values of thermal and cool waters are between −9.0 and −8.1‰ and between −51.8 and −58.9‰, respectively (Table 2) (Fórizs et al., 2011). The values indicate a meteoric origin for the waters with residence times of about 20–30 years (Şimşek, 2003). The R/RA and mantle-derived CO_2 are higher in the eastern part of Büyük Menderes Graben (Karakuş and Şimşek, 2013). The $\delta^{13}C$ analyses from the waters show that the CO_2 required for travertine deposition was derived largely from the decomposition of carbonate rocks (Filiz, 1984), along with a substantial contribution of magmatic CO_2.

4.3. Travertine mineralogy

Based on the XRD analysis of ~50 travertine samples, calcite is the most common mineral at all sites (Table 3). Aragonite and dolomite are, however, also present in the travertines found on the northern basin margin at Çukurbağ (Table 3, Figs. 10, 11) and Gölemezli, respectively. Although micrite (grains < 4 μm long) dominate most deposits, the vertically banded travertine, crystalline crusts and secondary pore fills are formed largely of coarse spar calcite (Figs. 11D, 12). The white, recently precipitated crystalline crust travertine (Fig. 12A–D), precipitated on the slope in front of Jandarma spring at Pamukkale, is formed mainly of dendritic calcite (Fig. 12D) (Jones and Kahle, 1986; see also Kele et al., 2011). There, minor amounts of aragonite (<1%) are also present on the distal part of the discharge apron. Some samples contain detrital minerals, including quartz, gypsum, mica, goethite, smectite and kaolinite in very small amounts (Table 3).

At Pamukkale and Çukurbağ, aragonite, in varying amounts, is associated with the vertically banded, ooid, and coated gas bubble travertine (Table 3; Figs. 10, 11, 13). A white, compact and finely crystalline crust sample (ÇB-6) (Fig. 10A) formed entirely of aragonite (Fig. 10A–D) was found adjacent to the orifice of Çukurbağ spring, where mesothermal waters are discharged at a temperature of 57 °C.

Some of the vertically banded travertine from the Çukurbağ fissure ridge (Fig. 11A) is formed by fibrous aragonite and rhombohedral calcite (Fig. 11B–D), each being segregated into alternating laminae, as confirmed also by cathodoluminescence analysis. Several aragonite samples from the fine crystalline crust and vertically banded travertines show rosette forms that are radially arranged (Fig. 10B–D).

Subrecent aragonite ooids, up to 8 mm in diameter (Fig. 13A, B), are found around the orifice of Çukurbağ spring. The concentric cortical laminae (Fig. 13C, D), 3 to 13 μm thick (Fig. 13E), are formed largely of aragonite needles that are up to 3 μm long (Fig. 12F). The ooids are held in calcite cement (Table 3). Goethite (<2%) is present in some of the iron-rich samples.

Some of the samples from Gölemezli contain up to 14% dolomite grains that are up 200 μm long (Fig. 14). The dolomite is typically found with quartz and mica grains (Fig. 14A, B) in mm-scale layers, lenses, and pockets that lie between calcite laminae (Fig. 14A). Some of the grains were removed from their places leaving behind mouldic cavities (Fig. 14C, D). This association of the dolomite with the quartz and mica indicates that it is probably of detrital origin.

4.4. Travertine geochemistry

4.4.1. Major and trace elements

Based on 55 samples that were analyzed geochemically (Table 4), the Ca concentrations in the travertines range from 329,857 to 405,214 ppm whereas the Mg varies from 120 ppm at Çukurbağ to 8160 ppm at Gölemezli (site 1). Calcite vein travertine at Gölemezli yielded Mg values of 20,940 ppm. The minimum and maximum Sr values in calcite are from Ballık (184 ppm) and Pamukkale (3028 ppm), respectively. Aragonite at Çukurbağ (Pamukkale-site 2), which comes from the vertically banded travertine (ÇB-6) along the central fissure of the Çukurbağ ridge, contains up to 7392 ppm Sr (Table 4).

Fe and Mn values of the calcite are lower in the light coloured travertines (e.g., ~280 ppm Fe, 70 ppm Mn, in the white crystalline calcite travertine precipitated on the slope facies of Pamukkale). The Fe (37,209 ppm) is high in the reddish-brown calcite from the Akköy travertine ridge (Table 4). The Mn content in the calcite is 1471 ppm from the dark brown coloured travertine from Ballık (site 3). In the same site, an abnormal Mn value of 27,640 ppm is from secondary enrichment in a cavity. Although there are some exceptions, basin-wide there is a positive correlation ($R^2 = 0.58$) between Fe and Mn (Table 4).

4.4.2. Stable carbon and oxygen isotope composition

The stable carbon ($\delta^{13}C$) and oxygen ($\delta^{18}O$) compositions of the travertine deposits, derived from 66 samples, vary from one site to another in the basin (Table 4, Fig. 15). The $\delta^{13}C$ values range from −4.0 to +11.7‰ PDB, whereas $\delta^{18}O$ values range from −16.6 to −7.8‰ PDB. Along the northern boundary (e.g., Gölemezli, Pamukkale, Çukurbağ, and Akköy) and around Kocabaş, the recent and fossil travertines have high $\delta^{13}C$ values (+3.7 to +11.7‰). In contrast, the lowest $\delta^{13}C$ values (−4.0‰) are from the tufas that are located along the southern boundary (e.g., Honaz) where both positive and negative values of the $\delta^{13}C$ have been measured. Similar $\delta^{13}C$ values (−3.3 to +0.8‰) were obtained from Kömürcüoğlu quarry, which is located east of the Ballık site (Table 4, Fig. 15).
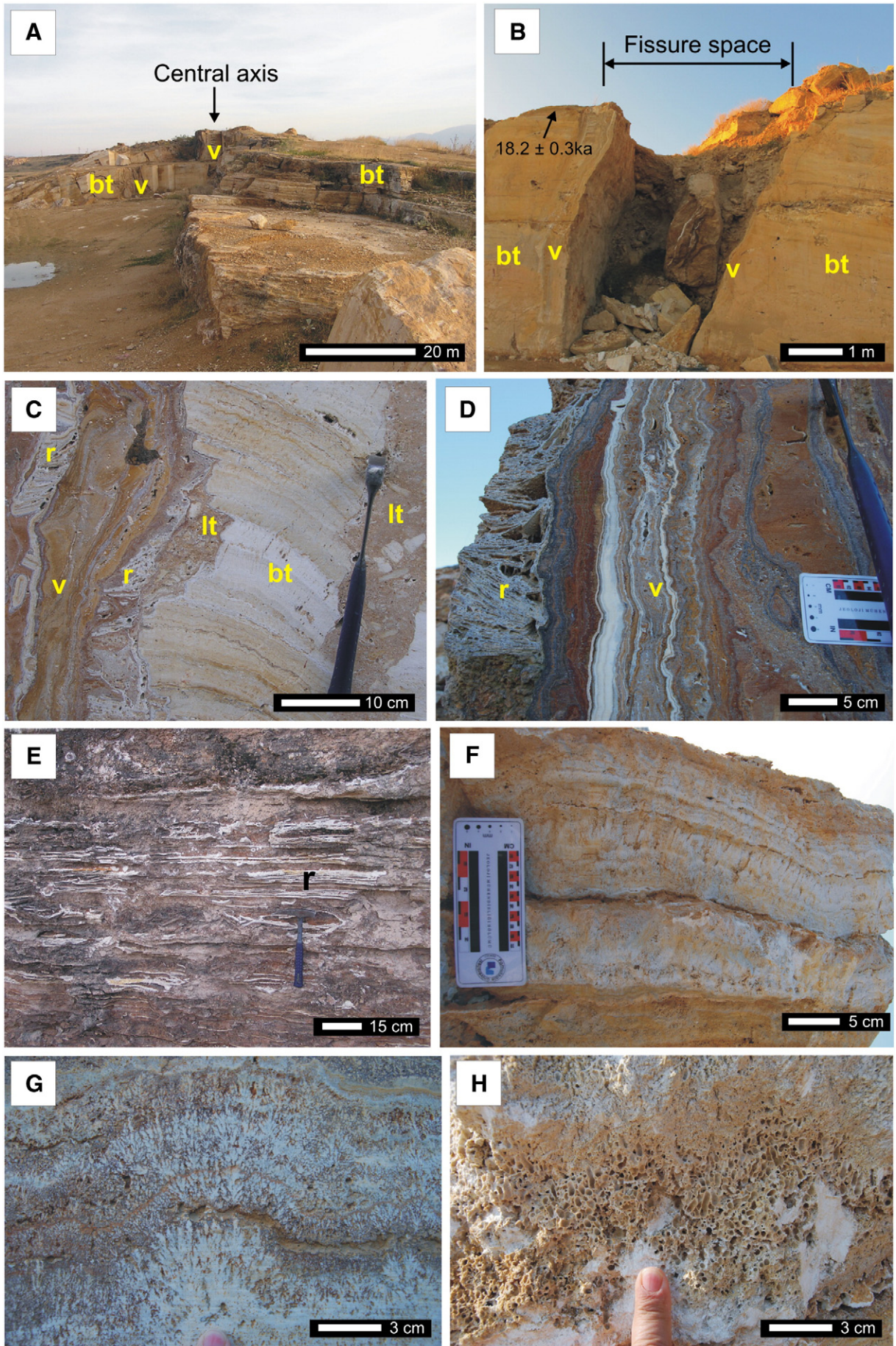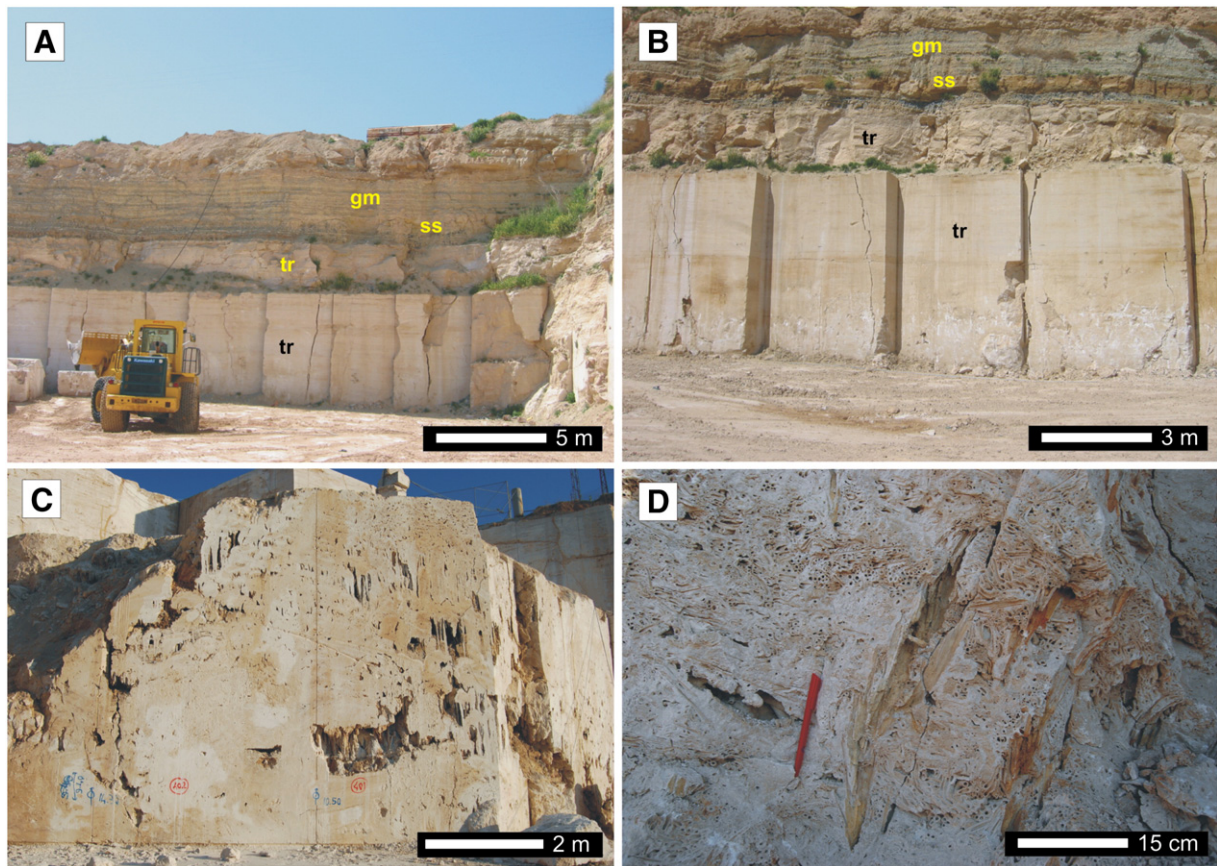
Fig. 6. Field photographs of Ballık site. (A) Horizontally bedded travertines (tr) at the bottom, overlain by green mudstones (gm) and sandstone (ss), west end of Çakmak quarry, southwest part of the area. (B) Close view of horizontally bedded travertines in A. (C) Tufa mound formed mainly of reed cluster with large cavities, quarry face is ~5.5 m high. (D) Reed casts, in growth position, in tufa mound.

5. Interpretation of data

5.1. Variations in depositional setting of the travertine

The depositional architecture of the travertines varies from locality to locality in accord with the conditions that existed at each site when the water was actively flowing. At Ballık, the horizontally bedded travertines, exposed in the lower part of the succession, grade upward into the low angle slope facies and then to the tufa horizon. The uppermost tufa horizon is a dome-like structure formed from numerous mound and waterfall bodies, which have coalesced with each other in all directions (Özkul et al., 2002). The mound facies is comparable to the 'reed mound facies' found in Rapolano Terme, Italy (Guo and Riding, 1998). The waterfall facies is similar to those found at other localities (Pedley et al., 2003; Özkul et al., 2010). The lower part of the succession formed in a shallow lake or depression environment that was fed by warm thermal waters that were modified by rainwater. This part of the succession is comparable to the travertines found at Tivoli, near Rome (Chafetz and Folk, 1984; Minissale et al., 2002; Faccenna et al., 2008), Rapolano Terme in Tuscany, central Italy (Guo and Riding, 1998), and Süttő, which is located on the Danube River, ~60 km northwest of Budapest, Hungary (Sierralta et al., 2010).

The recent travertines at Pamukkale have developed largely on smooth and terraced slope environments that are fed by warm thermal springs (T = ~34.5 °C at the spring orifice). Downslope variations in the thermal waters and associated precipitates are well documented (Ekmekçi et al., 1995; Şimşek et al., 2000; Kele et al., 2011). The slight downslope increase in the δD and $\delta^{18}O_{water}$ values is attributed to progressive evaporation (e.g., Fouke et al., 2000) and decrease in water temperature. The downslope increase in $\delta^{13}C_{travertine}$ is linked to the amount of CO_2 degassing (Kele et al., 2011).

Fissure ridges are one of the most prominent features in the region. They have been considered as important tools for tectonic investigations (Altunel and Hancock, 1993a,b; Hancock et al., 1999; Brogi and Capezzuoli, 2009; De Filippis et al., 2012) because local stress directions can be inferred from them (Hancock et al., 1999). At Pamukkale, for example, the east–west- and northwest–southeast-trending fissure ridges are products of local N–S and NE–SW stress directions, respectively.

Along the southern boundary of the basin, travertine and tufa deposits developed along the Honaz boundary fault. Travertines formed in these areas display slope and ridge-like depositional morphologies, whereas the tufa deposits are evident in the paludal and waterfall facies (Horvatinčić et al., 2005). The coexistence of tufa and travertine at adjacent localities at the western end of the Honaz fault probably

Fig. 5. Field photographs of travertines in the Akköy fisssure ridge showing which veins. Here bt: bedded travertine, lt: lithoclast, r: raft, and v: vein. (A) Cross-section view perpendicular to the central fissure axis. Bedded travertines gently dip away opposite sides with respect to the ridge axis in the middle. View from the northwest. (B) Fissure space, 3 m wide, bounded by vertical bands on both sides. (C) Multistage fissure fill with sharp contact. (D) Multistage vertical veins and raft clusters attached to the fissure wall. (E) Horizontal ledges (white) on fissure wall, resulting from progressive accumulation of rafts. (F) Bedded travertines composed of crystal shrubs. (G) Dendritic crystal shrub layers. (H) Coated gas bubbles in bedded travertines, north flank of Akköy fissure ridge.
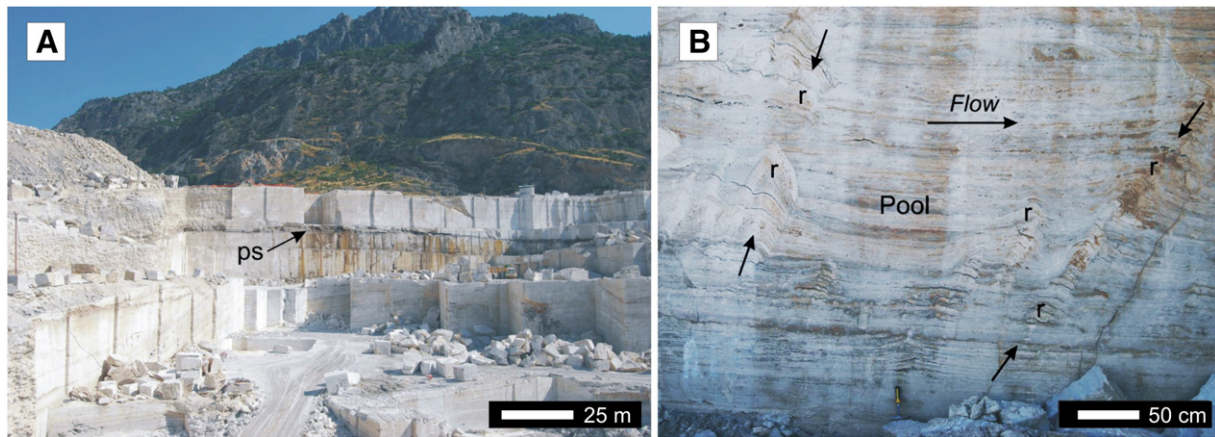
Fig. 7. Field photographs of Kelkaya site, situated at the foot of northern slope of the Kelkaya Hill. (A) Light coloured travertines were deposited on a gentle slope that prograded to the north. The uppermost bench (~12 m high) is underlain by a palaeosol layer (ps). Keltepe Hill, in the background, is composed of Mesozoic limestone. (B) Terrace pools and rims (r) on cut surface showing successive rims aligned on the same line (arrowed). Flow to the right.

resulted from shallow and deeply circulated waters in the fault damage zone (Brogi and Capezzuoli, 2009).

5.2. Occurrence of aragonite versus calcite

Precipitation of the calcite and aragonite found in these travertines was controlled by a complex set of interrelated parameters (Jones and Renaut, 2010). Aragonite and calcite precipitation depends on many factors including water temperature, growth inhibitors, supersaturation with respect to $CaCO_3$ caused by CO_2 degassing and/or evaporation (Chafetz et al., 1991), Sr content (Malesani and Vanucchi, 1975), Mg/Ca ratio (Folk, 1994), and various biological factors (Kitano, 1962; Busenburg and Plummer, 1986; Renaut and Jones, 1997; Pentecost, 2005; Jones and Renaut, 2010; Rodríguez-Berriguete et al., 2012). Based on a survey of spring deposits, Folk (1994) suggested that water temperature and the Mg:Ca ratio are the main controlling factors. Thus, he argued that aragonite is precipitated from waters with a temperature > 40 °C, whereas calcite precipitates when the temperature is <40 °C. There are, however, many exceptions. At Angel Terrace, Mammoth Hot Springs in Yellowstone National Park, for example, aragonite is precipitated at temperatures > 44 °C, whereas aragonite and calcite co-precipitate between 30 and 43 °C, and only calcite precipitates below 30 °C (Fouke et al., 2000). At Egerszalók, Hungary, where the water temperature is ~70 °C, almost pure calcite is precipitated around a borehole (e.g., spring vent), whereas farther downslope, various amounts of aragonite (5–35%) are being precipitated where the water temperatures are 45–50 °C (Kele et al., 2008). Similarly, calcite was precipitated directly from waters with temperatures of >90 °C in Kenya (Jones and Renaut, 1995) and New Zealand (Jones et al., 1996). In natural settings, identifying the factor(s) that control the precipitation of these polymorphs is difficult because all the environmental factors are operating simultaneously.

In the Denizli Basin, calcite is the dominant mineral found at all travertine sites. Aragonite is found in two different settings that clearly illustrate the diverse settings where aragonite can develop.

- Some of the banded travertines, found along fault planes and extensional fissures, are formed from alternating calcite and aragonite laminae. Uysal et al. (2007) showed that the aragonite and calcite found at Pamukkale were original precipitates with no evidence that the calcite had formed by inversion of the aragonite. In other springs, aragonite precipitation has been attributed to periods of rapid CO_2 degassing and the consequent high levels of supersaturation (Jones and Renaut, 2010). Occasionally, aragonites include needle aggregates, some of them may have microbial nuclei such as

bacteria and pollen, on which the needles grew (Guo and Riding, 1992). The aragonite in the fine crystalline crust- and vertically banded travertines examined in this study is formed from needle aggregates that do not appear to include any microbial nucleus (Fig. 10B–D). Spherulitic aragonite growth, without microbial nucleus, has been ascribed to high disequilibrium conditions (Jones and Renaut, 1995) or inorganic processes that include rapid CO_2 degassing (Pentecost, 1990).

- Aragonite ooids and crusts formed in and around the margin of the Çukurbağ hot spring pool. Similar aragonitic ooids, up to 5 cm in diameter, have also been reported from Tekkehamam (called as 'Tekke Ilıca' in Richter and Besenecker, 1983), close to Sarayköy town southwest of the Denizli Basin, which is one of the main geothermal fields in the Denizli province. There, aragonitic ooids may have formed from the thermal waters (up to 99.7 °C) that are of Na–SO₄–HCO₃ type (Şimşek, 2003), high supersaturation level (Sc: 0.6–0.7) with respect to $CaCO_3$, and rapid CO_2 degassing (Ali Gökgöz, unpublished data).

5.3. Occurrence of dolomite

Dolomite is rare in travertine. Barnes and O'Neil (1971) found dolomite in a few Californian travertines and trace amounts of dolomite have been found and in some of the Japanese (Kitano, 1963) and Italian hot springs (Folk, 1994). Minor amounts of dolomite were found with calcite and aragonite around hot spring orifices at Chemurkeu on the western shore of Lake Bogoria (Renaut and Jones, 1997).

In the Denizli Basin, dolomite was found in some of the banded travertine at Gölemezli along with quartz and mica grains. There, the underlying bedrocks are formed from dolomite and dolomitic limestone. The association of the dolomite with the quartz and mica suggests that the dolomite is probably of detrital origin.

5.4. Strontium distribution at the travertine sites

In the Denizli Basin, the Sr in the hot waters and travertines ranges from 1.16 to 9.09 ppm and 184 to 7392 ppm, respectively (Tables 2, 4). Travertines found at the northern sites (i.e., Gölemezli, Yenice, Karahayıt, Pamukkale, Çukurbağ and Akköy) contain more Sr than the travertines found in the east, southeast and south localities (i.e., Ballık, Kelkaya and Honaz). The highest Sr contents in the northern sites are from the vertically banded- and crystalline crust travertines. The Sr in the modern crystalline calcite travertines at Pamukkale decreases significantly from the proximal to distal areas on the slope aprons (Kele et al., 2011). A
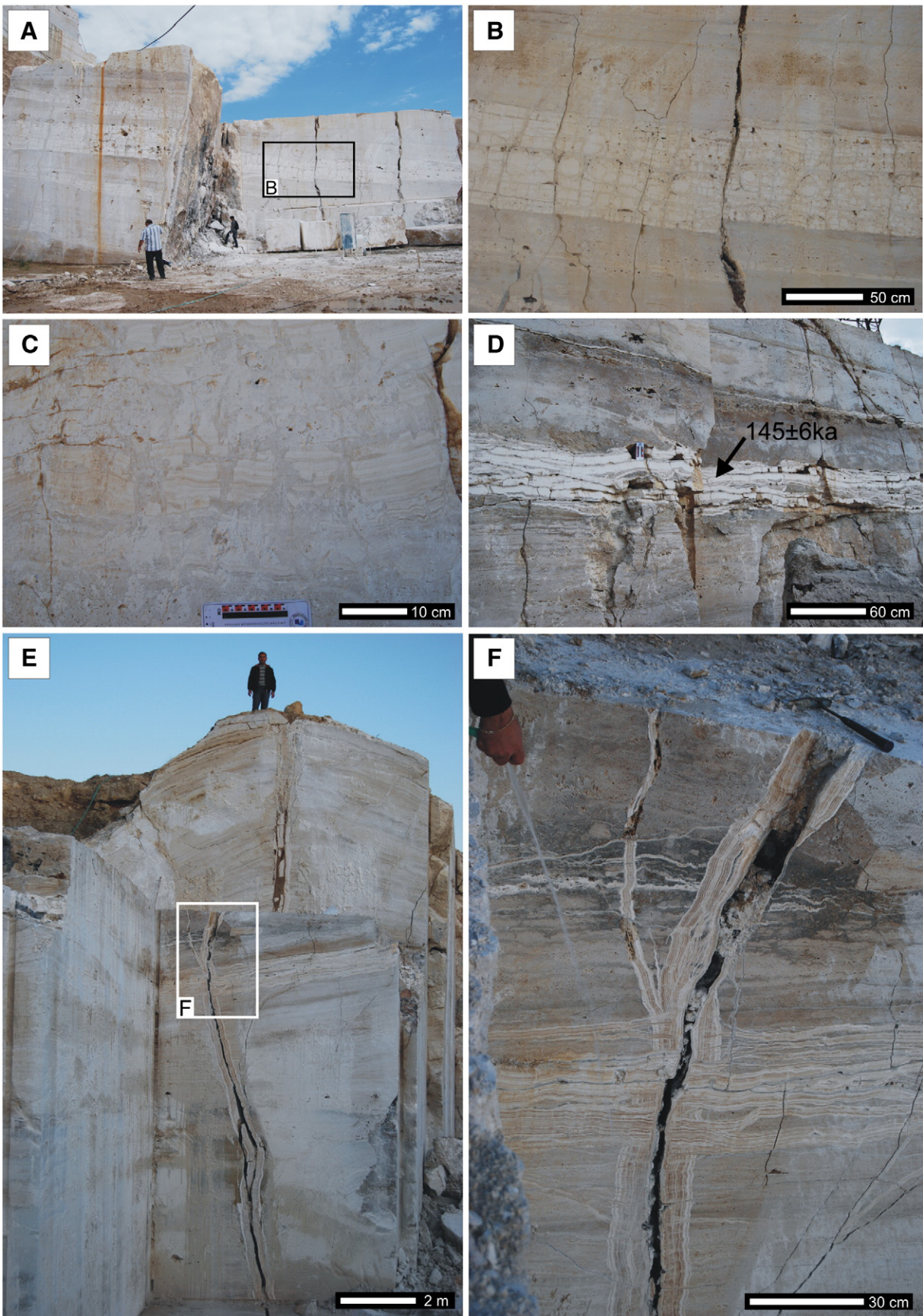
Fig. 8. Field photographs of crystalline vein travertines exposed in quarry faces around Kocabaş. (A) Light coloured, gently inclined crystalline beds, up to 60 cm in thickness, penetrated as an interlayer between the bedded travertines. Box labelled B indicates area shown in panel B. (B) Crystalline calcite bed in the inset area in A. (C) Brecciated crystalline vein travertine on the quarry face. (D) White crystalline vein beds penetrated along the bedding plane of the dark travertines. (E) Cross-cut relationship between the vertical and horizontal veins on quarry wall cut in fissure ridge, the Kuşgölü area, north of the Highway 320. Box labelled F indicates area shown in panel F. (F) Close view of the cross-cut relationship, inset area in E. Many vertical and horizontal veins cut of each other repeatedly.
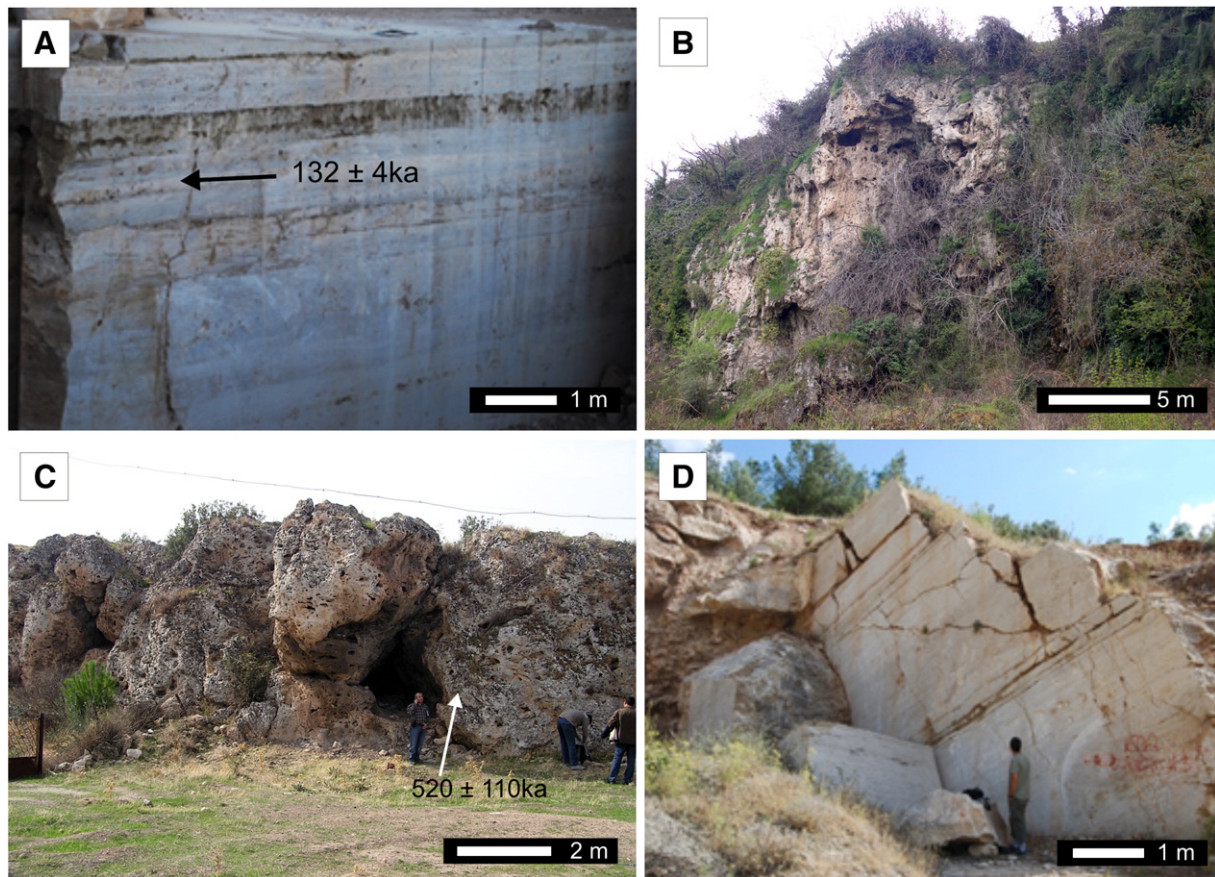
Fig. 9. Field photographs of the Gürlek and Honaz sites. (A) Light and dark coloured, horizontally bedded travertines with palaeosol horizon, quarry face (5 m high), near Gürlek, Kocabaş showing U–Th date. (B) Waterfall facies with hanging tufa curtain (~20 m high), Kayaaltı sublocality, west end of the Honaz fault zone, south of the basin. (C) Waterfall tufa exposure near the Karateke village, with a U–Th age of 520 ± 110 ka, west end of the Honaz fault zone. (D) Parallel bedded travertine sequence tilted to the southeast due to faulting, Gökpınar area, southwest boundary of the basin (see Fig. 1 for locations).

similar trend was reported from Angel Terrace, Mammoth Hot Springs (Yellowstone National Park, U.S.A.) (Fouke et al., 2000).

In central Italy, the Sr concentration of inactive travertines (up to 1500 ppm at Viterbo) and Sr concentration of present thermal springs are higher to the west of the Tiber Valley than those to the east (Minissale et al., 2002, their Fig. 8). The elevated concentration of Sr and SO_4 in thermal springs west of the Tiber Valley is probably caused by the interaction of the circulating groundwater with the gypsum in the Triassic Burano Formation found at the base of the Mesozoic limestone sequence (Minissale et al., 2002).

In the Denizli Basin, the Late Triassic Kızılyer Formation (Gündoğan et al., 2008), which is formed from evaporites and dolomites (Alçiçek et al., 2003), crops out as a tectonic slice at the eastern end of the Honaz fault near Kızılyer, may be the source of Sr found in the travertines. The deeply circulated thermal waters in the basin could have interacted with the buried part of the Kızılyer Formation. Some Sr may also have come from the Neogene strata in the Denizli Basin that includes gypsum intercalations in the areas around Sarayköy and Gölemezli (Alçiçek et al., 2007).

5.5. Basinal variations of the stable isotopic composition

Stable isotopic compositions of travertines have been linked to regional fluid flow, active tectonics, and palaeoenvironmental and palaeoclimatic changes during the Late Quaternary (Chafetz and Lawrence, 1994; Guo et al., 1996; Hancock et al., 1999; Uysal et al., 2007, 2009; Sierralta et al., 2010; Kele et al., 2011). For example,

there are consistent differences in the geochemical and isotopic signatures of modern and fossil travertines, associated thermal spring waters, and gas vents found on the east and west sides of Tiber Valley (central Italy). On the west side of Tiber valley, $\delta^{13}C$ values of fossil travertines are higher than those to the east side (e.g., the Ancona–Anzio line). Fossil travertines to the east have characteristics typical of meteogene origin (e.g., tufa including abundant plant casts and organic impurities) (Minissale et al., 2002).

In the Denizli Basin, the stable isotope compositions of the travertine deposits show some variations based on the location within the basin. The $\delta^{13}C$ values of recent and fossil travertines found along the northern boundary (i.e., Pamukkale, Karahayıt and Gölemezli) yielded more positive $\delta^{13}C$ values than those from the other sites (Table 4, Fig. 15A). More positive $\delta^{13}C$ values like these have been attributed to the contribution of CO_2 liberated by thermometamorphic processes associated with magmatic activity (Kele et al., 2011). The shift in the $\delta^{13}C$ values, up to + 11.7‰ PDB, are thought to arise from the more rapid CO_2-degassing that was associated with the fast flowing water on the steeper parts of the downslope sections (Kele et al., 2011). In contrast, the less positive and more negative values obtained from other precipitates possibly resulted from mixing between deeply sourced CO_2 and soil-derived CO_2 (Crossey et al., 2006).

5.6. Palaeotemperature calculations

Calcite oxygen isotope palaeothermometry generally uses equations that implicitly assume equilibrium isotope fractionation during
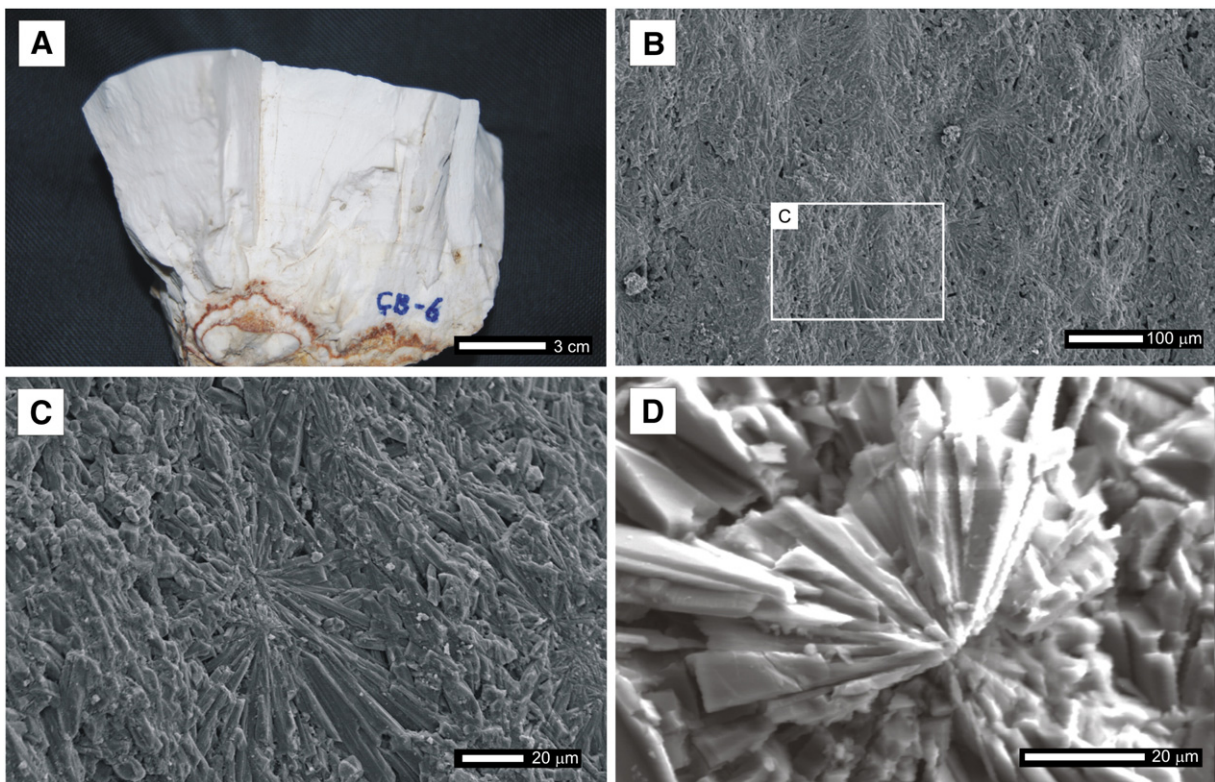
Fig. 10. (A) Dense, white aragonite crust (sample ÇB-6) from Çukurbağ hot spring orifice, Pamukkale. (B) SEM image of aragonite rosettes from the ÇB-6 sample. Box labelled C indicates area shown in panel C. (C) Area formed from radially arranged aragonite crystals. (D) Aragonite rosette from vein travertine, Çukurbağ fissure ridge.

carbonate precipitation (e.g., Friedman and O'Neil, 1977 [Eq. (1)], Kim and O'Neil, 1997 [Eq. (2)]):

$$10^3 \ln\alpha_{c-w} = \left(2.78 \times 10^6\right)/T^2 - 2.89 \qquad (1)$$

$$10^3 \ln\alpha_{c-w} = 18030/T - 32.42 \qquad (2)$$

where $\alpha = (\delta^{18}O_{calcite} + 1000) / (\delta^{18}O_{water} + 1000)$ and $10^3\ln\alpha_{c-w} \approx \delta^{18}O_{calcite} - \delta^{18}O_{water}$.

For these equations, palaeotemperature calculations are based on the $\delta^{18}O_{calcite}$ values and the $\delta^{18}O_{water}$. In the case of fossil travertine deposits, however, the $\delta^{18}O_{water}$ is not known and must therefore be inferred. This is further complicated by the fact that isotopic equilibrium is rarely maintained under natural conditions (e.g., Coplen, 2007; Kele et al., 2008; Demény et al., 2010; Tremaine et al., 2011). At Pamukkale, for example, there is a systematic positive shift in the Δ(calcite-water) values downslope (Kele et al., 2011). For travertines precipitated around spring orifices, deviation from the equilibrium can cause the calculated temperature to be 8–9 °C lower than the true temperature (Kele et al., 2011). Most of the samples are composed of calcite. Some samples, like those from Çukurbağ and Kocabaş (Table 3), however, contain significant up to 100% aragonite (Table 3). Zhou and Zheng (2003), Kim and O'Neil (2005), and Kim et al. (2007) showed that the difference between calcite-water and aragonite-water fractionation can produce a bias of up to 5 °C (Kele et al., 2008). Herein, palaeotemperature calculations (Table 5) were based on the equilibrium equations of Friedman and O'Neil (1977) and Kim and O'Neil (1997) and modified using the observations of Kele et al. (2011). For these the calculations, we used $\delta^{18}O_{water}$ values of recent springs that are located closest to the travertine body and it was assumed that the oxygen isotope composition of the palaeosprings was similar to those of the current springs.

At Pamukkale, it was possible to test the reliability of the equilibrium equations (Eqs. (1), (2)) for palaeotemperature calculations, because there are recent deposits and the parent waters allow comparison of the measured and calculated temperatures of deposition (Kele et al., 2011, their Fig. 16). These samples showed that the use of the Friedman and O'Neil (1977) and Kim and O'Neil (1997) equilibrium equations produced underestimations of 4.2–7.1 °C compared to the real (observed) temperature (Table 5). This demonstrates that precipitation of the calcite was not in isotopic equilibrium with the spring waters.

The highest calculated temperatures came from Gölemezli (51–73 °C), Çukurbağ (37–69 °C) and Kocabaş (47–56 °C), whereas medium temperatures came from Akköy fissure ridge (26–45 °C) and Ballık (23–39 °C), and the lowest temperatures came from Honaz (22–30 °C) and Kelkaya (22–26 °C). These temperature ranges are based on all $\delta^{18}O_{travertine}$ values because it is generally impossible to precisely locate the orifice of palaeospring systems. For the fissure ridge systems, samples from the central part of the ridge should be located closest to the orifice and should provide the highest palaeotemperature data. In other words, samples providing the highest calculated palaeotemperatures (Table 5) could have been precipitated from the warmest waters (i.e., closest the orifice of the palaeospring).

Using the U–Th age of the travertines and comparing the temperature of the current springs with the calculated temperature values of the palaeosprings a slight overall decrease in the average temperature of the hydrothermal system seems to have taken placed between the Pleistocene and the Holocene. It should be noted, however, that the $\delta^{18}O_{water}$ values of the palaeosprings could have been 3‰ lower than the recent ones during glacial periods. If so, the calculated temperatures would be high.

5.7. Origin of the banded travertines

The banded (or vein) travertines, one of the most important components of the travertines in the Denizli Basin, typically fill spaces
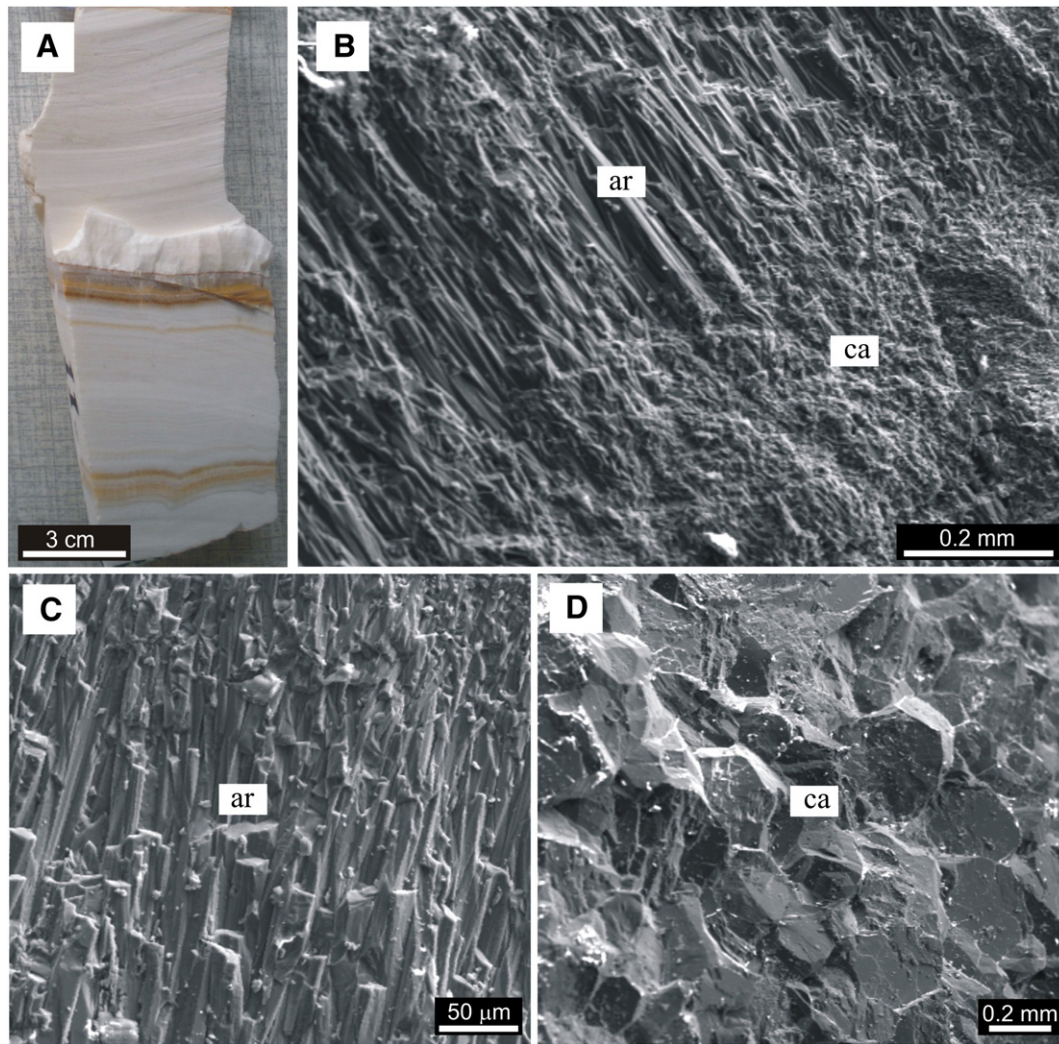
Fig. 11. Hand specimen photo and SEM images of vertically banded travertine sample (ÇB-11a) from Çukurbağ fissure ridge, Pamukkale. (A) White and brown layers on cut surface formed from calcite and aragonite in different ratio, confirmed by XRD measurements. (B) Alternation of fibrous aragonite (ar) and rhombohedral calcite (ca) layers. Close views of (C) fibrous aragonite and (D) rhombohedral calcite crystals.

along the normal fault planes and fissure spaces that are found in the travertine ridges (Altunel and Hancock, 1993a,b; Hancock et al., 1999; Özkul et al., 2002). The best examples are found in the Çukurbağ and Akköy fissure ridges around Pamukkale, Gölemezli and Yenice to the north–northwest and at Kocabaş to the east. In some cases, they are found as veins that cut across bedded travertines and bedrocks (Rihs et al., 2000; Uysal et al., 2009). They are composed of calcite and/or aragonite.

The vein travertines with high Sr content (up to 6822 ppm, Table 4) are typically found closest to linear spring discharges along the fissures. The high Mg content (4560 to 8160 ppm) of the Gölemezli samples (Table 4) is probably related to the detrital dolomite that came from the underlying dolomitic bedrock. The $\delta^{13}C$ values of the vein travertines, compiled from this study and others (Uysal et al., 2007; De Filippis et al., 2012), are highly positive ($+3.7$ to $+5.8‰$) (Fig. 15A, B; Supplementary Table 1) and display a uniform distribution for each locality as in Gölemezli, Çukurbağ, Akköy and Kocabaş where the $\delta^{18}O$ values range from $+13.8$ to $19.5‰$ (Fig. 15B). Similar ranges of values were obtained from vein deposits at Pamukkale and in the Gediz graben (Uysal et al., 2007, their Fig. 2). The positive $\delta^{13}C$ values of the vein travertines have been attributed to a thermogene origin (Uysal et al., 2007, 2009). Data obtained in this study indicate that many of the other lithotypes are also of thermogene origin (Table 4, Fig. 15A, B). According

to Uysal et al. (2007), the banded travertines may have been generated by rapid precipitation from meteoric waters that were enriched in CO_2 of deep origin and mobilised during intense seismic activity.

5.8. Geochronology of the travertine occurrences and possible influence of palaeoclimate on precipitation

Although the number of qualitative and quantitative data for the ages of the travertines in the Denizli Basin has increased (Altunel, 1996; Özkul et al., 2004; Altunel and Karacabak, 2005; Erten et al., 2005; Uysal et al., 2007; Kappelman et al., 2008; Uysal et al., 2009; De Filippis et al., 2012), the age of the earliest travertine deposition and the complete chronology of different travertine occurrences remain debatable. Nevertheless, compilation all the age data from this study (Table 1) and previous works allows comparison between development of the springs in the Denizli with global and regional palaeoclimate trends (Fig. 16, Supplementary Table 2).

The travertine deposits are located at elevations ranging from 1092 m north of Ballık (site 3) to 370 m near Kocabaş (site 5). A travertine sample from the elevation of ~1000 m at Ballık gave a thermoluminescence (TL) age of 510 ± 50 ka (Özkul et al., 2004), whereas one from a lower elevation (~370 m) near Gürlek (site 5a) yielded an U–Th age of 108.7 ± 2.0 ka. Likewise, an U–Th age of the travertine sample OT-3
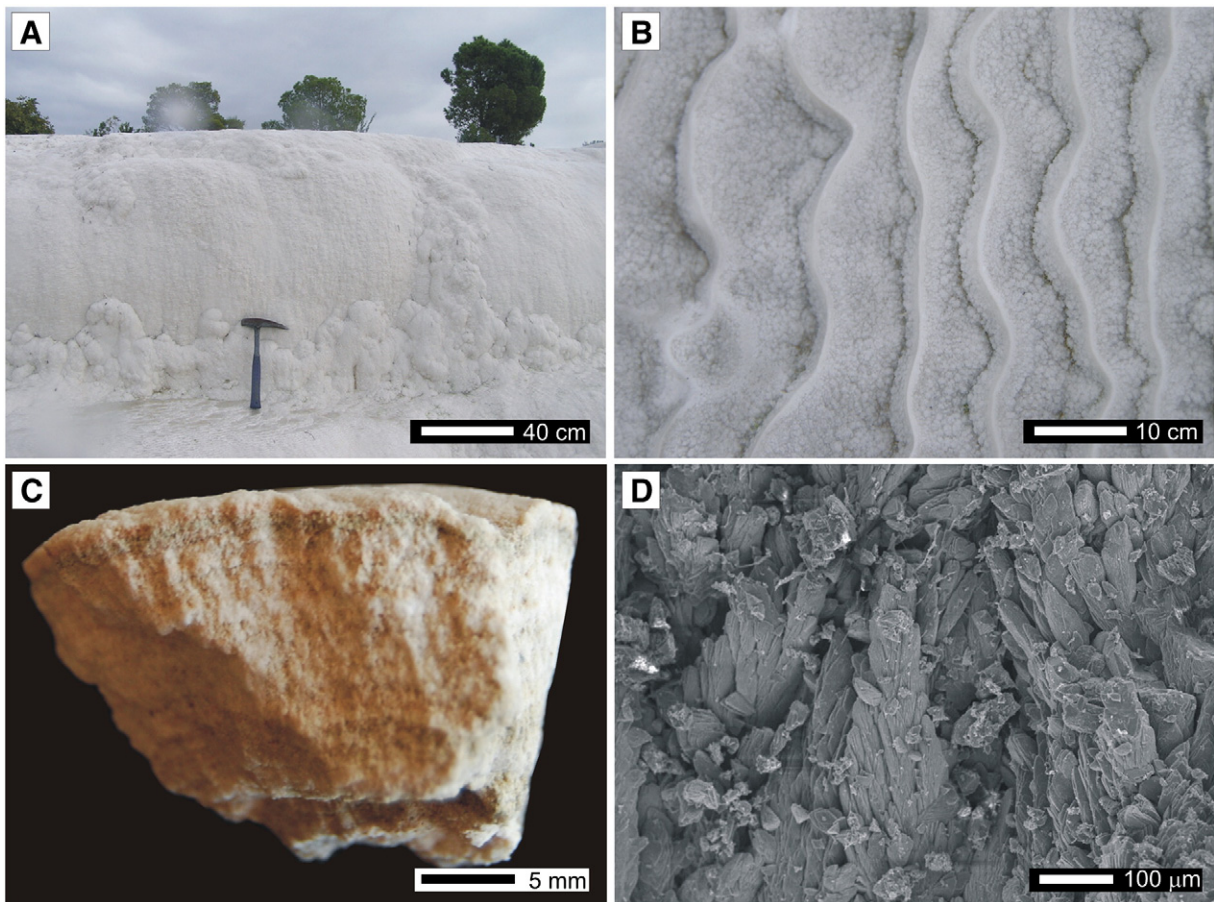
Fig. 12. (A) Front surface of rimstone dam formed from crystalline calcite, proximal slope in front of Jandarma spring, Pamukkale. Length of the hammer: 32 cm. (B) Microterrace pools developed on the proximal slope in front of Jandarma spring, Pamukkale. (C) Hand specimen of modern crystalline crust travertine developed perpendicular to the depositional surface (sample PK-12). (D) SEM image from sample PK-12 shown in panel C. The calcite dendrites are in growth position.

from Obruk hill (510 m asl), near Karateke (site 6a) is 544 ± 111 ka. These ages indicate that the travertine deposition becomes younger from the graben's margins north and south towards the centre. It should be noted, however, that in some localities (e.g., Pamukkale) travertine deposition was active during many different time intervals (Fig. 16).

There is only limited number of palaeoclimate records for the Late Quaternary in Turkey (Nicoll and Küçükuysal, 2013). Thus, the high resolution records derived from the marine benthic record (Lisiecki and Raymo, 2005), the speleothems from the eastern Mediterranean region and China (Bar-Matthews et al., 1999, 2003; Wang et al., 2001, 2008), and the combined records of Peqiin and Soreq speleothems in Israel (Bar-Matthews et al., 2003) have been used in an effort to decipher the relationship between travertine deposition and palaeoclimate in the study area.

In this study, fifteen travertine samples have been U–Th dated (Table 1). The oldest age of 613 ka came from Gölemezli (site 1), whereas the youngest age came from Akköy ridge. Another vein sample from Gölemezli yielded an age of 345 ± 18 ka, which corresponds to marine isotope stage (MIS) 10. The high error margin associated with this sample, however, means that it could partly overlap into MIS 9 (Fig. 16).

Fifty-eight age dates are available for Pamukkale (site 2) and its associated subsites (e.g., Çukurbağ and Akköy) with those greater than 400 ka (Fig. 16, Supplementary Table 2) being obtained from some of the banded travertines and 'eroded sheet travertines' (Altunel, 1994, 1996). The U–Th dates spanning the 18 to 25 ka time interval match dry and cold period of MIS 2 (Uysal et al., 2009; De Filippis et al., 2012). This time period is characterized by ^{18}O-enriched values in

cave records from the eastern Mediterranean region (Bar-Matthews et al., 1999, 2003; Fleitmann et al., 2009) and mainland China (Wang et al., 2001, 2008).

Eight samples with ages between 27.5 and 58.31 ka coincide with the younger $\delta^{18}O$ part of MIS 3. One bedded travertine sample from Çukurbağ with a U–Th age of 60 ± 1 ka (De Filippis et al., 2012) corresponds to the lower boundary of MIS 4.

Nineteen banded/vein samples from the fissure ridges at Pamukkale (Altunel and Karacabak, 2005; Uysal et al., 2007) yielded ages between 72.5 ± 0.9 and 124.3 ± 15 ka (Fig. 16, Supplementary Table 2). This group matches with MIS 5 as recorded from the Peqiin Cave stalagmite, north Israel (Bar-Matthews et al., 2003). In addition, four ages (e.g., 108.7 ± 2, 114 ± 10, 128.8 ± 3.8, 232 ± 27 ka) from the bedded travertines at Gürlek (site 5a) near Kocabaş (Table 1) indicate that precipitation took place during MIS 5 and MIS 7. This case implied that some veins at the Kocabaş area formed after surface travertine deposition had ceased at Gürlek. According to data presently available, travertine deposition in the Denizli Basin took place during glacial and interglacial palaeoclimate periods (Fig. 16). These data indicate that travertine deposition during the late Quaternary was not strongly influenced by climatic variations.

6. Discussion

The depositional architecture and geochemical characteristics of the travertine deposits are controlled by the balance between extrinsic (e.g., tectonics, seasonal climatic variations) and intrinsic (e.g., composition and flow pattern of spring water) factors (Jones and Peng, 2012).
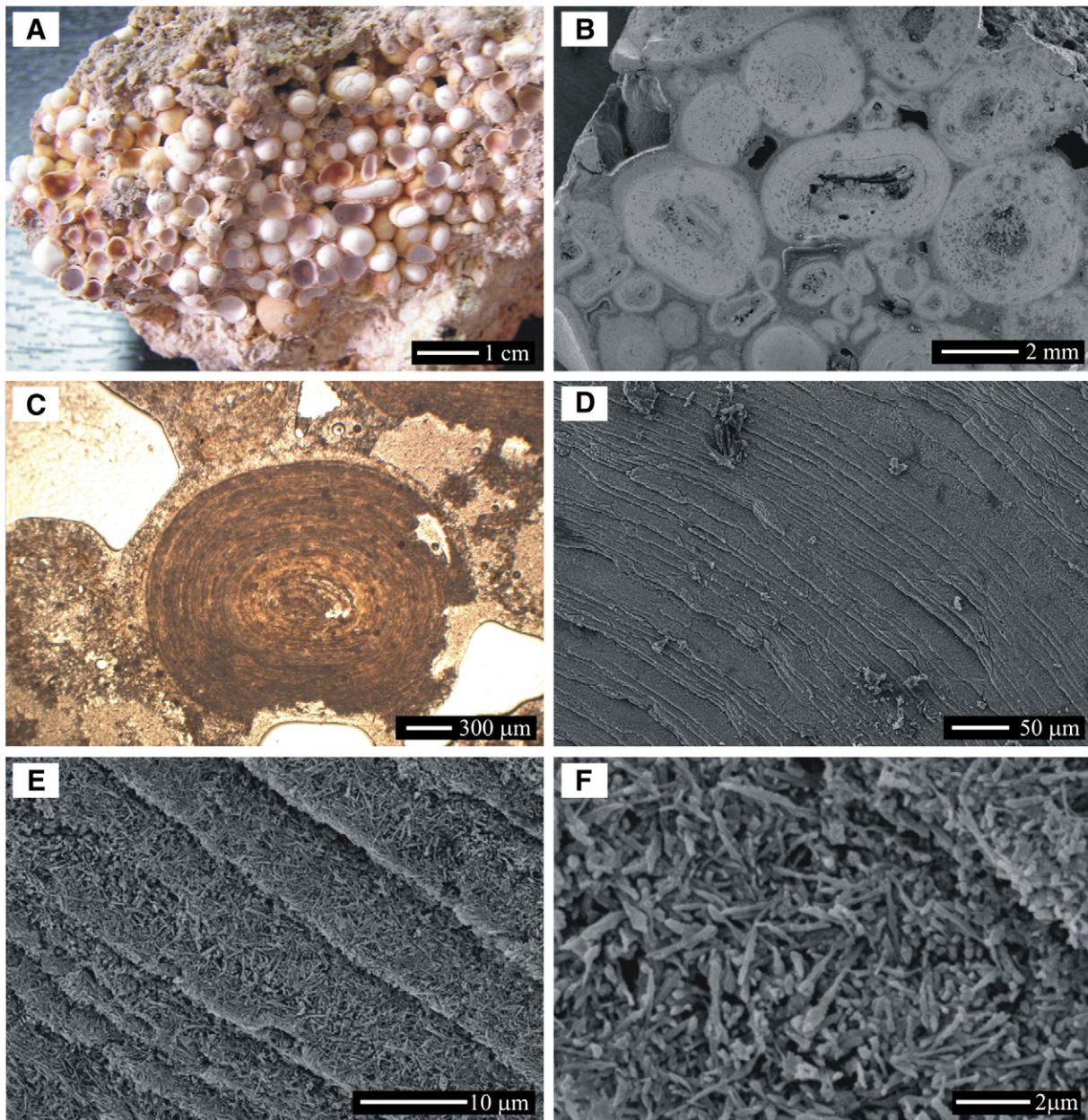
Fig. 13. Aragonite ooids from Çukurbağ, Pamukkale. (A) Hand specimen of the ooids, precipitated from bubbling mesothermal waters of 58 °C in Çukurbağ spring orifice. (B) SEM image of concentrically laminated ooids in different size. Some grains, ranging in shape from spherical through irregularly rounded, have been subjected to plastic deformation. (C) Thin section image of a single ooid displaying regular concentric lamination, formed in bubbling water. (D) Close view of concentric laminae. (E) Concentric laminae, up to 12 μm thick, composed of aragonite needles. (F) Close view of aragonite needles with sizes of 2–3 μm.

These factors, which operate over all scales and vary through time, are collectively responsible for the tufa and travertine that form around spring vents (Guo and Riding, 1998; Minissale et al., 2002; Jones and Renaut, 2010). To separate the effect that each of these factors may have had on the development of ancient travertines is, however, difficult. One possible way of doing this is to compare different travertine deposits that occur in a single basin like the Denizli extensional basin (Fig. 1).

The Denizli Basin, which is one of the main geothermal provinces in Turkey (Ekmekçi et al., 1995; Şimşek, 2003; Mutlu et al., 2008), is still seismically active today (Ates and Bayülke, 1982; Altunel and Barka, 1996). In this region, the upper crust is cut by numerous water saturated cracks and fluid pressure is high (Kaypak and Gökkaya, 2012). High mountains to the north and south are the main recharge areas for the hydrothermal system (Özler, 2000) and the deep- and shallow sourced waters in the basin are mainly of meteoric origin (Table 2). As the thermal waters ascend to the surface, they mix with the shallow cool groundwater (Dilsiz, 2006; Crossey et al., 2009). The CO_2 involved in travertine precipitation comes from thermometamorphic processes associated with magmatic sources in the area (e.g., Kele et al., 2011).

Thermal waters (Group I, II) that come to the surface along the northern boundaries (e.g., Karahayıt, Pamukkale and Çukurbağ) are derived from deeply sourced waters, i.e. endogenic waters mixed with meteoric water in different ratios (Crossey et al., 2006; Fórizs et al., 2011), and have high water temperature, high amounts of free CO_2, and high saturation levels (Table 2). The waters in Karahayıt, Çukurbağ and Kelkaya springs are below saturation level with respect to calcite (Table 2) but become saturated as CO_2 degasses from the water while it flows downslope (Kele et al., 2011). In this part of the basin, travertines precipitated from hot waters of Group I, II and
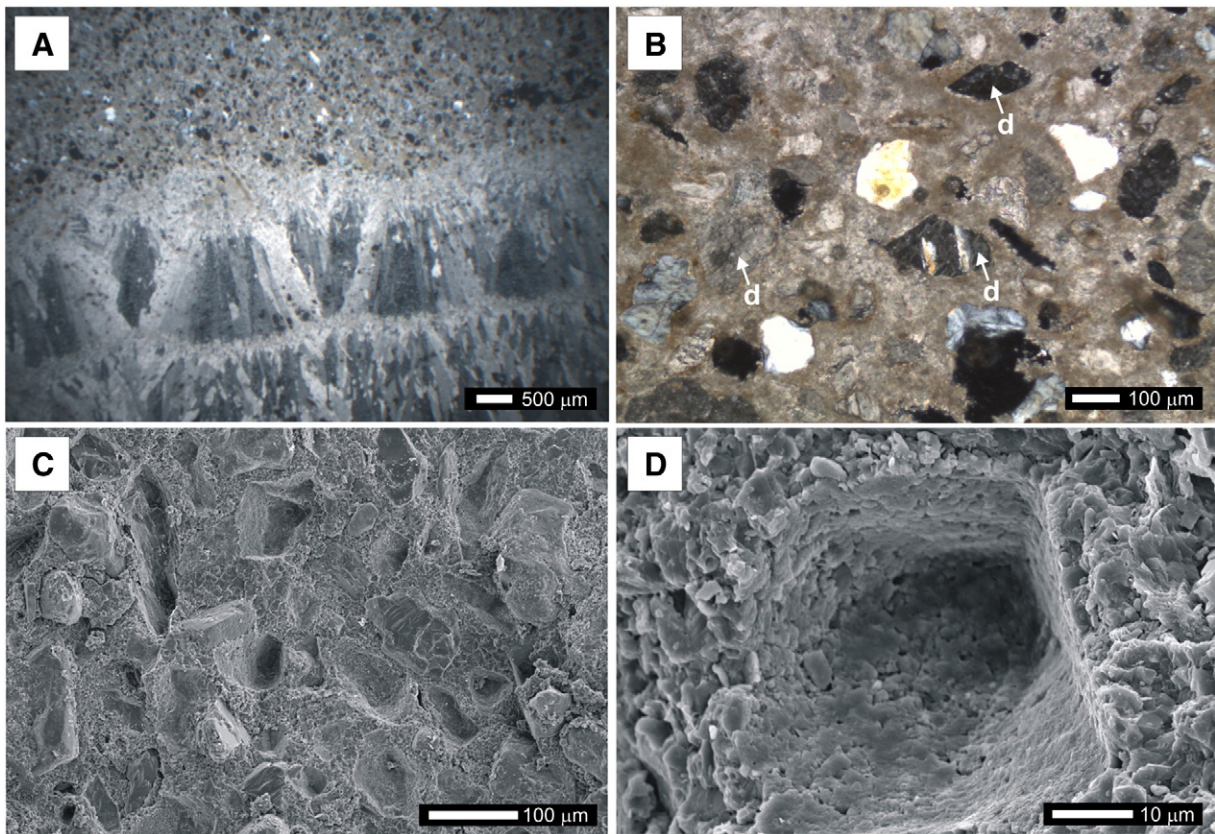
Fig. 14. Thin section and SEM images of the vein travertine (sample GL-20) from Gölemezli. (A) Thin calcite laminae with thickness of 1.0–1.5 mm below the sandy layer formed mainly of detrital dolomite, quartz, and mica. (B) Enlarged thin section image from the sandy field in A including detrital dolomite (d) arrowed. (C) Moulds appeared after removing a sand size grain. (D) A close view from one of the moulds in C.

fossil equivalents (i.e., Karahayıt and Pamukkale) have higher $\delta^{13}C$ and Sr values than the others (Tables 2, 4), and are composed mostly of calcite with only small amount of aragonite locally (Table 3).

The spring waters in Group III and IV (Table 2) to the east, southeast, and south (i.e., Kaklık cave, Kelkaya and Honaz), with low temperature (~19–24 °C) and high discharge rates, are characterized by groundwater circulation and mixing at shallow depths (Gökgöz, 1998; Horvatinčić et al., 2005; Dilsiz, 2006). Tufa and travertine precipitates that formed during different time periods are found along the southern boundary at the western end of the Honaz fault (Table 1). These variations in travertine and tufa precipitation may reflect temporal variations in water supply, water chemistry, mixture of deeply derived endogenic waters and epigenic waters, CO_2 levels, tectonic/seismic activity and/or climatic controls (Jones and Peng, 2012).

In extensional and transtensional provinces, faults and associated fissures served as natural conduits for emerging thermal waters (Altunel and Hancock, 1993a; Hancock et al., 1999; Şimşek, 2003; Dilsiz, 2006; Brogi and Capezzuoli, 2009; De Filippis et al., 2012). Consequently, tectonic activity can significantly influence the depositional architecture of travertine precipitation at regional and local scales. At a local scale, various depositional morphologies exist (e.g., slope, waterfall, depression fill, fissure ridge, channel) during a particular period of time. Along boundary faults, the thermal springs emerge directly onto the slopes and lead to the formation of smooth and terraced slope deposits like those seen at Pamukkale and Kelkaya (Özkul et al., 2002; Kele et al., 2011). In these settings, dendritic calcite is commonly precipitated as the CO_2-rich spring water rapidly degases during their flow downslope (Kele et al., 2011; Jones and Peng, 2012). Similar modern and fossil examples of slope depositional systems have been reported from Mammoth Hot Spring in Yellowstone

National Park, Wyoming (Chafetz and Folk, 1984; Pentecost, 1990; Fouke et al., 2000), Rapolano Terme, central Italy (Guo and Riding, 1998), and the Denizli Basin (Özkul et al., 2002; Kele et al., 2011).

Warm springs, like those at Ballık (site 3), which produced the largest travertine deposit over a volume of ~0.94 km³, are characterized by horizontally bedded travertines that were precipitated in depressions and/or large pools.

Similarly, warm spring waters issuing into depressions resulted in laterally extensive deposits, like those found at Bagni di Tivoli, east of Rome (Chafetz and Folk, 1984; Faccenna et al., 2008) and Rapolano Terme (Guo and Riding, 1998). These deposits have been described as 'shallow lake-fill travertines' (Chafetz and Folk, 1984). In those deposits, steepening (evolving from depression to slope facies) and/or levelling upward (evolving from slope to depression or from mound to depression depositional systems) are possible (Guo and Riding, 1998).

At Ballık, the travertine sequence gradually evolved from a depression depositional system, represented by horizontally bedded travertines (Özkul et al., 2002), to a slope depositional system that was characterized by low angle smooth slope facies and waterfall or cascade facies (cf., Guo and Riding, 1998). The depression system that evolved upwards into slope deposition (cf., Guo and Riding, 1998) has been attributed to increased flow rates that caused an increase in deposition that promoted transformation of the area into a slope system (Jones and Renaut, 2010).

Fissure ridges are elongate, wedge like structures that formed as travertine was precipitated from hot waters that ascended along a fracture or fault plane (Altunel and Hancock, 1993a; Guo and Riding, 1999; Hancock et al., 1999; Atabey, 2002; Pentecost, 2005; Brogi and Capezzuoli, 2009; Selim and Yanik, 2009; De Filippis et al., 2012). The hydrostatic pressure needed to form the largest mounds
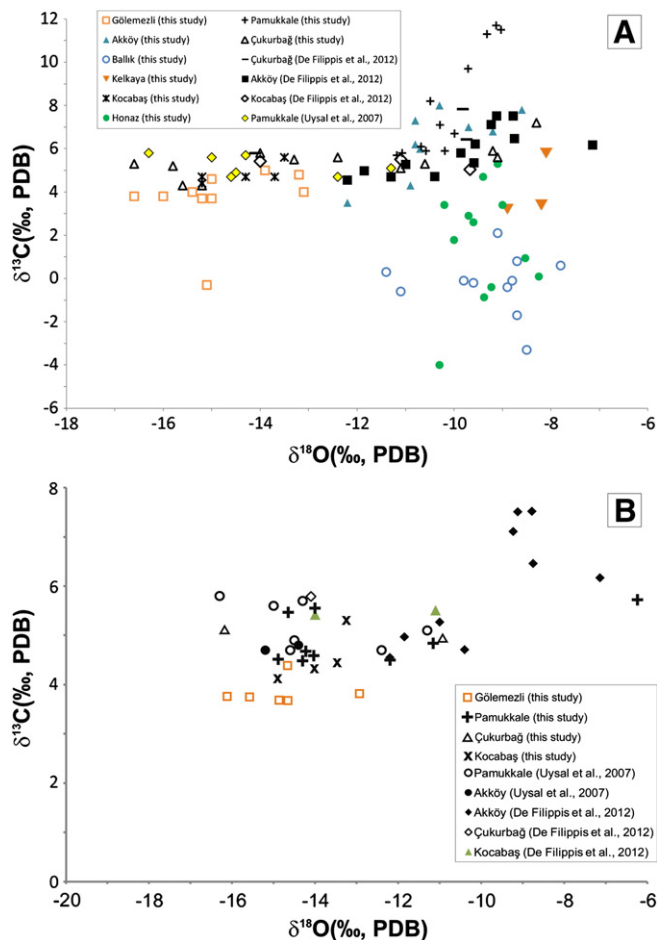
Fig. 15. (A) Basin scale distribution of stable carbon and oxygen isotope compositions of travertine samples in the Denizli Basin. (B) Stable carbon and oxygen isotope compositions of vein travertines. See Supplementary Table 1 for complete list of data. Data from this study (Table 4) are from Uysal et al. (2007) and De Filippis et al. (2012).

is considerable, approaching 7 kg cm^{-2} at ground level. These pressures, however, can be realised in artesian systems. Mound height must be limited by hydrostatic head. High supersaturation levels lead to rapid deposition around the vent and development of a steep mound (Pentecost, 2005).

The fissure ridges in the Denizli Basin are typically found at the ends of normal fault segments, which are step over or releasing zones, comprising a fracture network that are natural pathways for thermal waters (Çakır, 1999; Özkul et al., 2002; Altunel and Karabacak, 2005). These configurations are common along the northern boundary (e.g., Yenice and Pamukkale) and the Kocabaş area to the east (Fig. 1). In these areas, the physicochemical parameters like temperature, pCO_2, saturation level with respect to $CaCO_3$ of the present springs, and Sr are higher than those at other sites (Table 2). Maximum travertine deposition takes place along the central axis, possibly because of rapid CO_2 degassing that maintains the high levels of supersaturation with respect to $CaCO_3$. A hot spring, located at the eastern end of the Çukurbağ fissure ridge near Pamukkale (Fig. 4), for example, has the highest temperature, saturation levels, and Sr of all springs that were examined (Table 2). The formation of the banded travertines, however, is open to debate. Uysal et al. (2009) suggested that banded travertine formed during dry, cold periods and De Filippos et al. (2012) argued that they may have been formed from deep geothermal waters that had been released during seismic activity. Data compiled during this study, however, show that formation of the banded travertines cannot be attributed to specific climate conditions because they developed equally under cold, dry conditions and warm, wet conditions (Fig. 16). Some other

studies have also shown that vein travertines formed during warm periods, such as those that existed during MIS 1, MIS 5, and MIS 7 (Rihs et al., 2000; Kampman et al., 2012). In summary, the available data shows that travertine deposition in the Denizli Basin was probably caused by episodic fluxes in the deeply derived CO_2 that was related primarily to seismicity as a consequence of neotectonic activity (Crossey et al., 2011).

The highest calculated palaeotemperatures came from deposits found in the northern (e.g., Gölemezli, Çukurbağ) and eastern (around the Kocabaş fissure ridges) areas, whereas medial temperatures came from the Akköy fissure ridge and Ballık sites, and the lowest temperatures came from Honaz and Kelkaya sites in the south (Table 5). Overall, there appears to have been a slight decrease in the average temperature of the hydrothermal system from the Pleistocene to the Holocene. Palaeotemperature values show a similar distribution with respect to those of some other parameters (i.e., stable isotope, pCO_2, Sr, saturation level).

7. Conclusions

Quaternary travertine deposits of the Denizli extensional basin have been studied and compared in six locations with the view of determining the extrinsic and intrinsic factors that influenced their genesis. Travertine deposits in these locations, with thickness from 30 to 75 m, each cover an area between 1 and 34 km^2. Up to 1 km^3 of travertine volume is present in the largest deposit found at Ballık.

Today, spring waters found in the northern part of the Denizli Basin have the highest temperatures, electrical conductivity, dissolved CO_2, Sr, and $CaCO_3$ saturation levels. Collectively, the data indicate that these waters probably have deeper flow paths than elsewhere in the basin.

The travertines were precipitated in various depositional settings, including fissure ridges, slope systems, and depression systems. The fissure ridges, one of the main depositional morphologies, are restricted largely to the northern boundary. Present day travertine deposition continues on the terraced and smooth slopes at Pamukkale. The depression (or lake-fill) travertines are widespread around Ballık in the northeast. In this area, the depositional system evolved progressively from a horizontal depression, to low angle slope travertines, and finally to mound and waterfall systems at the top.

Although calcite is the dominant mineral at all sites, aragonite is present in some of the vertical banded, crystalline crust, raft and pisoid travertines from the Çukurbağ site (Pamukkale) in the north. The aragonite bearing samples rich in Sr are found mostly around the spring orifices. There are considerable variations in the stable isotope compositions of travertines throughout Denizli Basin. The $\delta^{13}C$ values of travertines found along the northern boundary are more positive than elsewhere (up to +12‰ PDB). Vein travertines precipitated in the fissure spaces and fractures of bedrocks, with a narrow range in $\delta^{13}C$ values from +3.7 to +5.8‰ (PDB) for each locality, display more uniform conditions during the precipitation. In contrast, the $\delta^{18}O$ values have a wide range.

The travertines have been precipitated in warm and wet periods as well as in cold and dry periods. The spring activity and therefore travertine precipitation in the Denizli Basin is not related to climate and appears to be largely a function of tectonic activity. Palaeotemperature calculations, similar to the present case, show higher values for the spring waters at the northern locations. However, from Pleistocene to Holocene a slight overall decreasing has been recorded in the spring temperatures.

Supplementary data to this article can be found online at http://dx.doi.org/10.1016/j.sedgeo.2013.05.018.

Table 5

Comprehensive table of palaeotemperature calculations for Denizli travertines including the stable oxygen isotope compositions of travertines and thermal springs.

Site name	Travertine δ18O (SMOW)	Water δ18O (SMOW)	Calc.[1] T(°C)	Calc.[2] T(°C)	Calc.[3] T(°C)	Calc.[4] T(°C)	T of recent Springs T(°C)	Travertine type	Aragonite (%)	(AGE) (ka)
Gölemezli (1)	14.5	−7.7	60	57	68	50	54.8	Vertically banded		611.230±∞
	13.8	−7.7	65	62	73	54		Vertically banded		
	17.4	−7.7	43	41	51	35		Vertically banded		
	15.2	−7.7	56	53	64	46		Vertically banded		
	15.5	−7.7	54	52	62	44		Vertically banded		
	15.4	−7.7	54	52	62	45		Vertically banded		
	16.6	−7.7	47	45	55	39		Bedded		
	17.3	−7.7	43	45	51	35		Bedded		
	15.1	−7.7	56	54	64	46		Raft		
Cukurbag (2)	14.8	−8.3	54	52	62	45	58	Crytalline crust	100	
	16.5	−8.3	44	43	52	36		Raft	5	
	17.2	−8.3	40	39	48	33		Raft, coated gas bubble	78	
	15.2	−8.3	52	50	60	43		Ooid		
	14.6	−8.3	56	53	64	46		Vertically banded	7-23	
	13.8	−8.3	61	58	69	50		Vertically banded		25.321±308
	19.5	−8.3	29	27	37	23		Vertically banded	70	
Akköy (3)	18.1	−8.1	37	35	45	30	53	Raft		
	20	−8.1	27	26	35	22		Brown		
	21.5	−8.1	20	19	28	16		Bedded		
	21.4	−8.1	21	19	29	16		Raft and micritic layer		
	19.6	−8.1	29	28	37	23		Bedded		
	20.3	−8.1	26	24	34	20		Bedded		18.188±314
	19.8	−8.1	28	27	36	22		bedded		
	20.9	−8.1	23	22	31	18		bedded		
	19.7	−8.1	29	27	37	23		Taft and micritic layer		
	22.1	−8.1	18	16	26	13		Bedded		
Ballik (4)	22	−8.1	18	16	26	14	22.8	Rimstone, Kaklik cave		
	21.8	−8.1	19	17	27	14		Dark coloured trav.		
	22.1	−8.1	18	16	26	13		Reddish-brown coloured		
	22.8	−8.1	15	13	23	11		Light coloured bedded		
	21.8	−8.1	19	17	27	14		Light coloured bedded		
	19.5	−8.1	30	28	38	24		Light coloured bedded		
	19.2	−8.1	31	30	39	25		Light coloured bedded		
	21	−8.1	23	21	31	17		Light coloured bedded		
	21	−8.1	23	21	31	17		Light coloured bedded		
	21.9	−8.1	19	17	27	14		Light coloured bedded		
	20.9	−8.1	23	22	31	18		Light coloured bedded		
Kocabas (5)	17	−8.8	39	37	47	31	23.7	Vertically banded	75	90.463±2645
	15.3	−8.8	48	46	56	40		Vertically banded	7	144.908±6287
	16.8	−8.8	40	38	48	32		Vertically banded		
	16.2	−8.8	43	42	51	35		Vertically banded		
Kelkaya (6)	22.4	−8.5	15	13	23	10	19.6	Bedded		
	22.6	−8.5	14	12	22	10		Bedded		
	21.7	−8.5	18	16	26	13		Bedded		
Honaz (7)	20.3	−8.8	22	21	30	17	20.2; 24; 18.8	Karateke, passive tufa		
	21	−8.8	19	18	27	15		Karateke, passive tufa		
	20.9	−8.8	20	18	28	15		Karateke, Honaz		
	21.2	−8.8	18	17	26	14		Karateke, Işik Tr. Quarry		
	21.2	−8.8	18	17	26	14		Değirmenler, recent tufa		
	21.4	−8.8	18	16	26	13		recent waterfall+moss		
	20.5	−8.8	21	20	29	16		Soft passive tufa		
	22.3	−8.8	14	12	22	10		Soft passive tufa		
Pamukkale (8)	19.9	−8.8	24	23	32		.30.1	Recent crystalline crust		recent
Pamukkale (9)	19.3	−8.5	29	27	37		33.2	Recent crystalline crust		recent

For the calculations the equilibrium equations of Friedman and O'Neil (1977) and Kim and O'Neil (1997) were used and was modified based from Kele et al. (2011). Temperature of recent thermal springs is also indicated for comparison, together with the travertine types, aragonite content and radiometric age of the deposits. Calculated maximum temperature values are highlighted with grey background. For the calculations the δ18O values of the following recent springs (data from Table 2) were used: (1) Gölemezli Şanlıalp, (2) Çukurbağ spring, (3) Karahayit Belediyesi well, (4) Kaklik cave, (5) Pınarbaşı warm well, (6) Kelkaya spring, (7) Pınarbaşı spring, (8) Pamukkale, Jandarma spring, (9) Pamukkale, Beltes-2 spring. Calculated maximum temperature values are highlighted with grey background.

Calc.[1] is based on Friedman and O'Neil (1977).

Calc.[2] is based on Kim and O'Neil (1997).
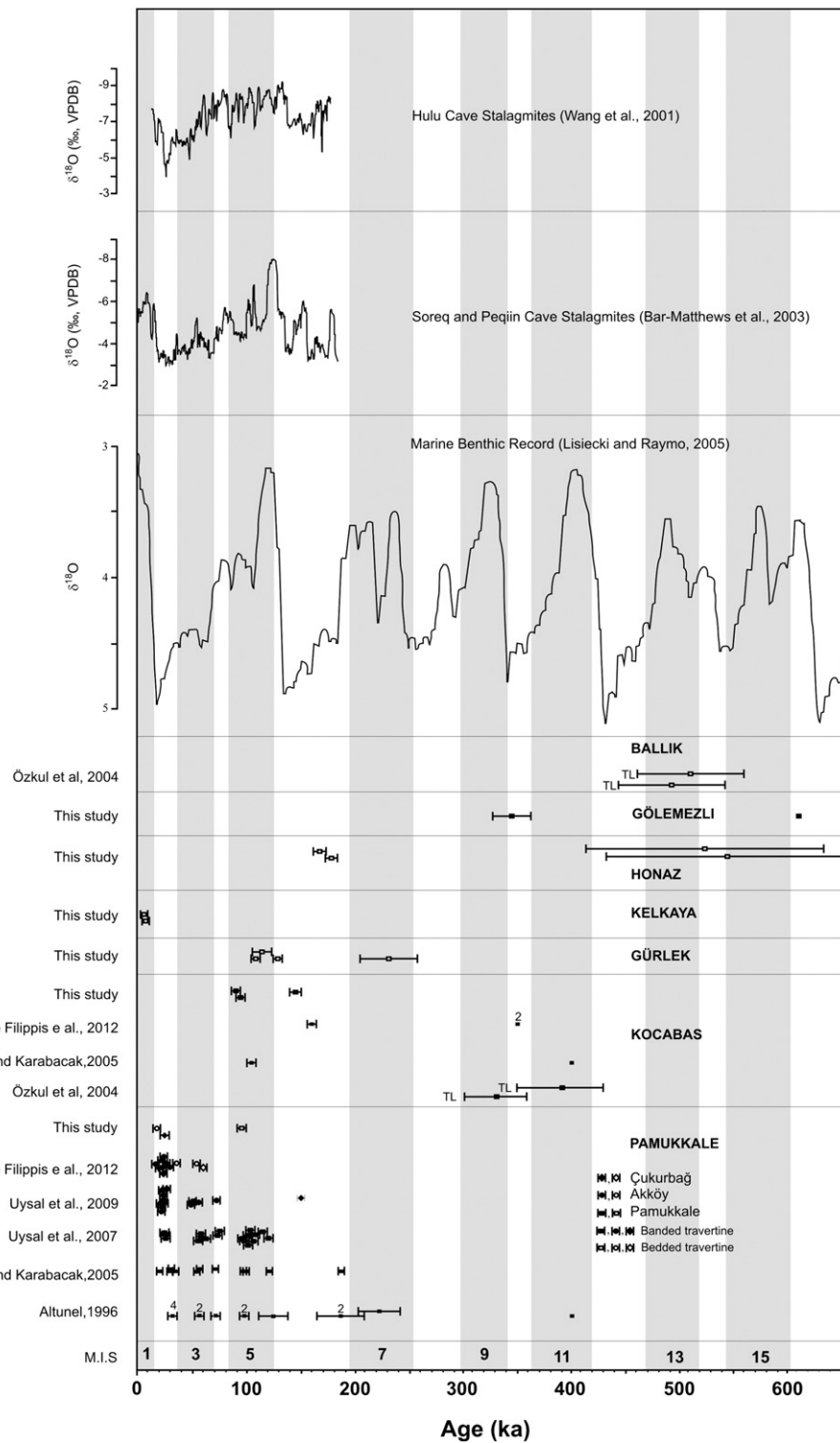
Calc.[3] is modified based from Kele et al. (2011).

Fig. 16. Comparison of U–Th ages of the travertine deposits from the Denizli Basin with regional and global palaeoclimate records. High δ^{18}O values are from stalagmites from Hulu and Soreq caves (Wang et al., 2001; Bar-Matthews et al., 2003). Age data from this study are combined with those from previous works (Altunel, 1996; Özkul et al., 2004; Altunel and Karabacak, 2005; Uysal et al., 2007, 2009; De Filippis et al., 2012). Global glacial periods (white bars and even numbers) and interglacial periods (shaded bars and odd numbers) are shown by marine isotope stages (MISs) which are from Lisiecki and Raymo (2005).

References

Alçiçek, H., Özkul, M., Varol, B., 2003. Elementary sulphur formation in Kızılyer evaporites and fissure fill gypsum (Denizli, SW Anatolia). 14th International Petroleum and Natural Gas Congress and Exhibition of Turkey, Proceedings, pp. 86–94.

Alçiçek, H., Varol, B., Özkul, M., 2007. Sedimentary facies, depositional environments and palaeogeographic evolution of the Neogene Denizli Basin of SW Anatolia, Turkey. Sedimentary Geology 202, 596–637.

Altunel, E., 1994. Active Tectonics and the Evolution of Quaternary Travertines at Pamukkale, Western Turkey. (Unpublished Ph.D. Thesis) University of Bristol, United Kingdom (236 pp.).

Altunel, E., 1996. Pamukkale travertenlerinin morfolojik özellikleri, yaşları ve neotektonik önemleri. Maden Tetkik ve Arama Dergisi 118, 47–64 (in Turkish).

Altunel, E., Barka, A., 1996. Evaluation of archaeoseismic damages at Hierapolis. Geological Bulletin of Turkey 39, 65–74 (in Turkish).

Altunel, E., Hancock, P.L., 1993a. Morphology and structural setting of Quaternary travertines at Pamukkale, Turkey. Geological Journal 28, 335–346.

Altunel, E., Hancock, P.L., 1993b. Active fissuring, faulting and travertine deposition at Pamukkale, western Turkey. In: Stewart, I.S., Vita-Finzi, C., Owen, L.A. (Eds.), Neotectonics and Active Faulting: Zeitschrift für Geomorphologie, Supplement, 94, pp. 285–302.

Altunel, E., Karacabak, V., 2005. Determination of horizontal extension from fissure-ridge travertines: a case study from the Denizli Basin, southwestern Turkey. Geodinamica Acta 18, 333–342.

Andrews, J.E., 2006. Paleoclimatic record from stable isotopes in riverine tufas: synthesis and review. Earth-Science Reviews 75, 85–104.

Andrews, J.E., Riding, R., Dennis, P.F., 1997. The stable isotope record of environmental and climatic signals in modern terrestrial microbial carbonates from Europe. Palaeogeography, Palaeoclimatology, Palaeoecology 129, 171–189.

Arenas, C., Gutiérrez, F., Osácar, C., Sancho, C., 2000. Sedimentology and geochemistry of fluvio-lacustrine tufa deposits controlled by evaporite solution subsidence in the central Ebro Depression, NE Spain. Sedimentology 47, 883–909.

Arenas-Abad, C., Vázquez-Urbez, M., Pardo-Tirapu, G., Sancho-Marcén, C., 2010. Fluvial and associated carbonate deposits. In: Alonso Zarza, A.M., Tanner, L.H. (Eds.), Carbonates in Continental Settings: Facies, Environments, and Processes: Development in Sedimentology, 61, pp. 133–175.

Atabey, E., 2002. Çatlak Sırt Tipi Laminalı Traverten-Tufa Çökellerinin Oluşumu, Mikroskobik Özellikleri ve Diyajenezi, Kırşehir, İç Anadolu. Maden Tetkik ve Arama Dergisi 123–124, 59–65 (in Turkish).

Ateş, R.C., Bayülke, N., 1982. The 19 August 1976 Denizli, Turkey, earthquake: evaluation of the strong motion accelerograph record. Bulletin of the Seismological Society of America 72, 1635–1649.

Aydan, Ö., Kumsar, H., Tano, H., 2005. Multiparameter changes in the earth's crust and their relation to earthquakes in Denizli region of Turkey. In: Row, B., Horne, R., Stacey, R., Juliusson, E., Villaluz, A., Chen, C.-Y., Dastan, A., Li, K., Garner, L., Bolds, J., Polyakova, J. (Eds.), Proceedings World Geothermal Congress, Antalya, Turkey, 24–29 April 2005, pp. 1–10 (on CD).

Bárdossy, Gy, Bottyán, L., Gadó, P., Griger, Á., Sasvári, J., 1980. Automated quantitative phase analysis of bauxites. American Mineralogist 65, 135–141.

Bar-Matthews, M., Ayalon, A., Kaufman, A., Wasserburg, G.J., 1999. The Eastern Mediterranean paleoclimate as a reflection of regional events: Soreq Cave, Israel. Earth and Planetary Science Letters 166, 85–95.

Bar-Matthews, M., Ayalon, A., Gilmour, M., Matthews, A., Hawkesworth, C.J., 2003. Sea-land isotopic relationships from planktonic foraminifera and speleothems in the Eastern Mediterranean region and their implication for palaeorainfall during inter-glacial intervals. Geochimica et Cosmochimica Acta 67, 3181–3199.

Barnes, I., O'Neil, J.R., 1971. Calcium–magnesium solid solutions from Holocene con-glomerate cements and travertines in the Coast Range of California. Geochimica et Cosmochimica Acta 35, 699–717.

Bozkurt, E., Oberhänsli, R., 2001. Menderes massif (Western Turkey): structural, metamor-phic and magmatic evolution — a synthesis. International Journal of Earth Sciences 89, 679–708.

Bozkuş, C., Kumsar, H., Özkul, M., Hançer, M., 2000. Seismicity of active Honaz fault under an extensional tectonic regime. In: Dora, O.Ö., Özgenç, İ., Sözbilir, H. (Eds.), Proceedings of International Earth Science Colloquium on the Aegean Region. Dokuz Eylül University, İzmir, Turkey, pp. 7–16.

Brogi, A., Capezzuoli, E., 2009. Travertine deposition and faulting: the fault-related travertine fissure-ridges at Terme S. Giovanni, Terme, Italy. International Journal of Earth Sciences 98, 931–947.

Busenberg, E., Plummer, L., 1986. A comparative study of the dissolution and crystal growth kinetics of calcite and aragonite. United States Geological Survey Bulletin 1578, 139–168.

Çakır, Z., 1999. Along-strike discontinuity of active normal faults and its influence on Quaternary travertine deposition: examples from western Turkey. Turkish Journal of Earth Sciences 8, 67–80.

Chafetz, H.S., Folk, R.L., 1984. Travertines: depositional morphology and the bacterially constructed constituents. Journal of Sedimentary Petrology 54, 289–316.

Chafetz, H.S., Lawrence, J.R., 1994. Stable isotopic variability within modern travertines. Géographie Physique et Quaternaire 48, 257–273.

Chafetz, H.S., Rush, P.F., Utech, N.M., 1991. Microenvironmental controls on mineralogy and habit of $CaCO_3$ precipitates: an example from an active travertine system. Sedimentology 38, 107–126.

Cheng, H., Edwards, R.L., Hoff, J., Gallup, C.D., Richards, D.A., Asmersom, Y., 2000. The half-lives of uranium-234 and thorium-230. Chemical Geology 169, 17–33.

Coplen, T.B., 2007. Calibration of the calcite-water oxygen-isotope geothermometer at Devils Hole, Nevada, a natural laboratory. Geochimica et Cosmochimica Acta 71, 3948–3957.

Crossey, L.J., Fischer, T.P., Patchett, P.J., Karlstrom, K.E., Hilton, D.R., Huntoon, P., Reynolds, A.C., 2006. Dissected hydrologic system at Grand Canyon: interaction between upper world and lower world waters in modern springs and travertine. Geology 34, 25–28.

Crossey, L.J., Karlstrom, K.E., Springer, A., Newell, D., Hilton, D., Fischer, T., 2009. Degassing of mantle-derived CO2 and 3He from springs in the southern Colorado Plateau region–neotectonic connections and implications for groundwater systems. Geological Society of America Bulletin 121, 1034–1053.

Crossey, L.J., Karlstrom, K.E., Newell, D.L., Kooser, A., Tafoya, A., 2011. The La Madera Travertines, Rio Ojo Caliente, Northern New Mexico: investigating the linked system of CO2-rich springs and travertines as neotectonic and paleoclimate indicators.

New Mexico Geological Society Guidebook, 62nd Field Conference, Geology of the Tusas Mountains — Ojo Caliente, pp. 121–136.

De Filippis, L., Faccenna, C., Billi, A., Anzalone, E., Brilli, M., Özkul, M., Soligo, M., Tuccimei, P., Villa, M., 2012. Growth of fissure ridge travertines from geothermal springs of Denizli Basin, western Turkey. Bulletin of the Geological Society of America 124, 1629–1645.

Demény, A., Kele, S., Siklósy, Z., 2010. Empirical equations for the temperature dependence of calcite-water oxygen isotope fractionation from 10 to 70 °C. Rapid Communications in Mass Spectrometry 24, 3521–3526.

Dilsiz, C., 2006. Conceptual hydrodynamic model of the Pamukkale hydrothermal field, southwestern Turkey, based on hydrochemical and isotopic data. Hydrogeology Journal 14, 562–572.

Ekmekçi, M., Günay, G., Şimşek, Ş., 1995. Morphology of rimstone pools, Pamukkale, western Turkey. Cave Karst Science 22, 103–106.

Erdoğan, B., Güngör, T., 2004. The problem of the core-cover boundary of the Menderes massif and an emplacement mechanism for regionally extensive gneissic granites, western Anatolia (Turkey). Turkish Journal of Earth Sciences 13, 15–36.

Erten, H., Sen, Ş., Özkul, M., 2005. Pleistocene mammals from travertine deposits of the Denizli basin (SW Turkey). Annales de Paléontologie 91, 267–278.

Faccenna, C., Soligo, M., Billi, A., De Filippis, L., Funiciello, R., Rossetti, C., Tuccimei, P., 2008. Late Pleistocene depositional cycles of the Lapis Tiburtinus travertine (Tivoli, Central Italy): possible influence of climate and fault activity. Global and Planetary Change 63, 299–308.

Filiz, S., 1984. Investigation of the important geothermal areas by using C, H, O isotopes. Seminar on the Utilization of Geothermal Energy for Electric Power Generation and Space Heating, 14–17 May 1984, Florence, Italy (Ref. No. EP/SEM.9/R.3).

Fleitmann, D., Cheng, H., Badertscher, S., Edwards, R.L., Mudelsee, M., Göktürk, O.M., Frankhauser, A., Pickering, R., Raible, C.C., Matter, A., Kramers, J., Tüysüz, O., 2009. Timing and climatic impact of Greenland interstadials recorded in stalagmites from northern Turkey. Geophysical Research Letters 36, L19707. http://dx.doi.org/10.1029/2009GL040050.

Folk, R.L., 1994. Interaction between bacteria, nannobacteria, and mineral precipitation in hot springs of Central Italy. Géographie Physique et Quaternaire 48, 233–246.

Ford, T.D., Pedley, H.M., 1996. A review of tufa and travertine deposits of the world. Earth-Science Reviews 41, 117–175.

Fórizs, I., Gökgöz, A., Kele, S., Özkul, M., Deák, J., Baykara, M.O., Alçiçek, M.C., 2011. Comparison of the isotope hydrogeological features of thermal and cold karstic waters in the Denizli Basin (Turkey) and Buda Thermal Karst (Hungary). Central European Geology 54 (1–2), 115–119.

Fouke, B.W., Farmer, J.D., Des Marais, D.J., Pratt, L., Sturchio, N.C., Burns, P.C., Discipulo, M.K., 2000. Depositional facies and aqueous-solid geochemistry of travertine de-positing hot springs (Angel Terrace, Mammoth Hot Springs, Yellowstone National Park, U.S.A.). Journal of Sedimentary Research 70, 565–585.

Friedman, I., O'Neil, J.R., 1977. Compilation of stable isotope fractionation factors of geochemical interest. United States Geological Survey KK1–KK12.

Gökgöz, A., 1994. Pamukkale-Karahayıt-Gölemezli Hidrotermal Karstının Hidrojeolojisi. (Unpublished Ph.D. thesis) Süleyman Demirel University, Isparta (263 pp.).

Gökgöz, A., 1998. Geochemistry of the Kızıldere–Tekkehamam–Buldan–Pamukkale geothermal fields. United Nations University, Geothermal Training Programme, Reports, Reykjavik, Iceland, pp. 115–156.

Gündoğan, İ., Helvacı, C., Sözbilir, H., 2008. Gypsiferous carbonates at Honaz Dağı (Denizli): first documentation of Triassic gypsum in western Turkey and its tectonic significance. Journal of Asian Earth Sciences 32, 49–65.

Guo, L., Riding, R., 1992. Aragonite laminae in hot water travertine crusts, Rapolano Terme, Italy. Sedimentology 39, 1067–1079.

Guo, L., Riding, R., 1998. Hot-spring travertine facies and sequences, Late Pleistocene Rapolano Terme, Italy. Sedimentology 45, 163–180.

Guo, L., Riding, R., 1999. Rapid facies changes in Holocene fissure ridge hot spring travertines, Rapolano Terme, Italy. Sedimentology 46, 1145–1158.

Guo, L., Andrews, J., Riding, R., Dennis, P., Dresser, Q., 1996. Possible microbial effects on stable carbon isotopes in hot-spring travertines. Journal of Sedimentary Research 66, 468–473.

Hancock, P.L., Chalmers, R.M.L., Altunel, E., Çakir, Z., 1999. Travitonics: using travertines in active fault studies. Journal of Structural Geology 21, 903–916.

Hancock, P.L., Chalmers, R.M.L., Altunel, E., Çakir, Z., Becher-Hancock, A., 2000. Creation and destruction of travertine monumental stone by earthquake faulting at Hierapolis, Turkey. In: McGuire, W.G., Griffiths, D.R., Hancock, P.L., Stewart, I.S. (Eds.), The Archae-ology of Geological Catastrophes: The Geological Society, London. Special Publications, 171, pp. 1–14.

Horvatinčić, N., Özkul, M., Gökgöz, A., Barešić, J., 2005. Isotopic and geochemical investi-gation of tufa in Denizli province, Turkey. In: Özkul, M., Yağız, S., Jones, B. (Eds.), Pro-ceedings of 1st International Symposium on Travertine, Kozan Ofset Matbaacılık. San. ve Tic. Ltd. Std, Ankara, pp. 162–170.

Jaffey, A.H., Flynn, K.F., Glendenin, L.E., Bentley, W.C., Essling, A.M., 1971. Precision measurement of half-lives and specific activities of U-235 and U-238. Physical Reviews 4, 1889–1906.

Jones, B., Kahle, C.F., 1986. Dendritic calcite crystals formed by calcification of algal filaments in a vadose environment. Journal of Sedimentary Petrology 56, 217–227.

Jones, B., Peng, X., 2012. Intrinsic versus extrinsic controls on the development of calcite den-drite bushes, Shuzhishi Spring, Rehai geothermal area, Tengchong, Yunnan Province, China. Sedimentary Geology 249–250, 45–62.

Jones, B., Renaut, R.W., 1995. Noncrystallographic dendrites from hot-spring deposits at Lake Bogoria, Kenya. Journal of Sedimentary Research 65, 154–169.

Jones, B., Renaut, R.W., 2008. Cyclic development of large, complex calcite dendrite crystals in the Clinton travertine, Interior British Columbia, Canada. Sedimentary Geology 203, 17–35.

Jones, B., Renaut, R.W., 2010. Calcareous spring deposits in continental settings. In: Alonso Zarza, A.M., Taner, L.H. (Eds.), Carbonates in Continental Settings: Facies, Environments, and Processes. : Developments in Sedimentology, 61. Elsevier, pp. 177–224.

Jones, B., Renaut, R.W., Rosen, M.R., 1996. High-temperature (>90 °C) calcite precipitation at Waikite Hot Springs, North Island, New Zealand. Journal of the Geological Society 153, 481–496.

Kampman, N., Burnside, N.M., Shipton, Z.K., Chapman, H.J., Nicholl, J.A., Ellam, R.M., Bickle, M.J., 2012. Pulses of carbon dioxide emissions from intracrustal faults following climatic warming. Nature Geoscience 5, 352–358.

Kappelman, J., Alçicek, M.C., Kazanci, N., Schultz, M., Özkul, M., Sen, S., 2008. Brief communication: first *Homo erectus* from Turkey and implications for migrations into temperate Eurasia. American Journal of Physical Anthropology 135, 110–116.

Karakuş, H., Şimşek, Ş., 2013. Tracing deep thermal water circulation systems in the E–W trending Büyük Menderes Graben, western Turkey. Journal of Volcanology and Geothermal Research 252, 38–52.

Kaymakçı, N., 2006. Kinematic development and paleostress analysis of the Denizli Basin (Western Turkey): implications of spatial variation of relative paleostress magnitudes and orientations. Journal of Asian Earth Sciences 27, 207–222.

Kaypak, B., Gökkaya, G., 2012. 3-D imaging of the upper crust beneath the Denizli geothermal region by local earthquake tomography, western Turkey. Journal of Volcanology and Geothermal Research 211–212, 47–60.

Kele, S., Demény, A., Siklósy, Z., Németh, T., Mária, T.B., Kovács, M., 2008. Chemical and stable isotope compositions of recent hot-water travertines and associated thermal waters, from Egerszalók, Hungary: depositional facies and non-equilibrium fractionations. Sedimentary Geology 211, 53–72.

Kele, S., Özkul, M., Gökgöz, A., Fórizs, I., Baykara, M.O., Alçiçek, M.C., Németh, T., 2011. Stable isotope geochemical and facies study of Pamukkale travertines: new evidences of low-temperature non-equilibrium calcite-water fractionation. Sedimentary Geology 238, 191–212.

Kim, S.-T., O'Neil, J.R., 1997. Equilibrium and nonequilibrium oxygen isotope effects in synthetic carbonates. Geochimica et Cosmochimica Acta 61, 3461–3475.

Kim, S.-T., O'Neil, J.R., 2005. Comment on "An experimental study of oxygen isotope fractionation between inorganically precipitated aragonite and water at low temperatures" by G.-T. Zhou and Y.-F. Zheng. Geochimica et Cosmochimica Acta 69, 3195–3197.

Kim, S.-T., Mucci, A., Taylor, B., 2007. Phosphoric acid fractionation factors for calcite and aragonite between 25 and 75 °C: revisited. Chemical Geology 246, 135–146.

Kitano, Y., 1962. A study of polymorphic formation of calcium carbonate in thermal springs with emphasis on the effect of temperature. Bulletin of the Chemical Society of Japan 35, 1980–1985.

Kitano, Y., 1963. Geochemistry of calcareous deposits found in hot springs. Journal of Earth Science, Nagoya University 11, 68–100.

Koçyiğit, A., 2005. The Denizli graben–horst system and the eastern limit of western Anatolian continental extension: basin-fill, structure, deformational mode, throw amount and episodic evolutionary history, SW Turkey. Geodinamica Acta 18, 167–208.

Lisiecki, L.E., Raymo, M.E., 2005. A Pliocene-Pleistocene stack of 57 globally distributed benthic δ18O records. Paleoceanography 20, 1–17.

Malesani, P., Vanucchi, S., 1975. Precipitazione di calcite o di aragonite dalle acque termominerali in relazione alla genesi e all'evoluzione dei travertini: Accademia Lincell, Rendiconti Scienze fisica, matematica e naturale, 58, pp. 761–776 (in Italian).

McCrea, J.M., 1950. On the isotopic chemistry of carbonates and a paleotemperature scale. Journal of Chemical Physics 18, 849–857.

Minissale, A., Kerrick, D.M., Magro, G., Murrell, M.T., Paladini, M., Rihs, S., Sturchio, N.C., Tassi, F., Vaselli, O., 2002. Geochemistry of Quaternary travertines in the region north of Rome (Italy): structural, hydrologic and paleoclimatologic implications. Earth and Planetary Science Letters 203, 709–728.

Mutlu, H., Gulec, N., Hilton, D.R., 2008. Helium–carbon relationships in geothermal fluids of western Anatolia, Turkey. Chemical Geology 247, 305–321.

Nicoll, K., Küçükuysal, C., 2013. Emerging multi-proxy records of late Quaternary palaeoclimate dynamics in Turkey and the surrounding region. Turkish Journal of Earth Sciences 22, 126–142.

Okay, A.I., 1989. Denizli'nin güneyinde Menderes masifi ve Likya naplarinin jeolojisi. Maden Tetkik ve Arama Dergisi 109, 45–48 (in Turkish).

Özkul, M., Varol, B., Alçiçek, M.C., 2002. Depositional environments and petrography of the Denizli travertines. Bulletin of the Mineral Research and Exploration 125, 13–29.

Özkul, M., Engin, B., Alçiçek, M.C., Koralay, T., Demirtaş, H., 2004. Thermoluminescence dating of Quaternary hot spring travertines and some implications on graben evolution, Denizli, Western Turkey. 32nd International Geological Congress, August 20–28, 2004, Florence, Italy.

Özkul, M., Gökgöz, A., Horvatinčić, N., 2010. Depositional properties and geochemistry of Holocene perched springline tufa deposits and associated spring waters: a case study from the Denizli province, Western Turkey. In: Pedley, H.M. (Ed.), Tufas and Speleothems: Unravelling the Microbial and Physical Controls: The Geological Society, London. Special Publications, 336, pp. 245–262.

Özler, H.M., 2000. Hydrogeology and geochemistry in the Çürüksu (Denizli) hydrothermal field, western Turkey. Environmental Geology 39, 1169–1180.

Parkhust, D.L., 1995. User's guide to PHREEQC—a computer program for speciation, reaction path, advective transport, and inverse geochemical calculations. U.S. Geological Survey Water Resources Investigations Report 95-4227 (143 pp.).

Pedley, H.M., 2009. Tufas and travertines of the Mediterranean region: a testing ground for freshwater carbonate concepts and developments. Sedimentology 56, 221–246.

Pedley, H.M., Ordonez, S., Gonzales-Martin, J.A., Garcia Del Cura, M.A., 2003. Sedimentology of Quaternary perched springline and paludal tufas: criteria for recognition, with examples from Guadalajara Province, Spain. Sedimentology 50, 23–44.

Pentecost, A., 1990. The formation of travertine shrubs: Mammoth Hot Springs, Wyoming. Geological Magazine 127, 159–168.

Pentecost, A., 2005. Travertine. Springer Verlag (446 pp.).

Piccardi, L., 2007. The AD 60 Denizli Basin earthquake and the apparition of Archangel Michael at Colossae (Aegean Turkey). In: Piccardi, L., Masse, W.B. (Eds.), Geological Society, London, Special Publications, 273, pp. 95–105.

Renaut, R.W., Jones, B., 1997. Controls on aragonite and calcite precipitation in hot spring travertines at Chemurkeu, Lake Bogoria, Kenya. Canadian Journal of Earth Sciences 34, 801–818.

Richter, D.V., Besenecker, H., 1983. Subrecent high-Sr aragonite ooids from hot springs near Tekke Ilica (Turkey). In: Perty, T.M. (Ed.), Coated Grains. Springer-Verlag, Berlin, pp. 154–162.

Rihs, S., Condomines, M., Poidevin, J.L., 2000. Long-term behaviour of continental hydrothermal systems: U-series study of hydrothermal carbonates from the French Massif Central (Allier Valley). Geochimica et Cosmochimica Acta 64, 3189–3199.

Rodríguez-Berriguete, A., Alonso-Zarza, A.M., Cabrera, M.C., Rodriguez-Gonzalez, A., 2012. The Azuaje travertine: an example of aragonite deposition in a recent volcanic setting, N Gran Canaria Island, Spain. Sedimentary Geology 277–278, 61–71.

Sant'Anna, L.G., Riccomini, C., Rodrigues-Francisco, B.H., Sial, A.N., Carvalho, M.D., Moura, C.A.V., 2004. The Paleocene travertine system of the Itaboraí basin, Southeastern Brazil. Journal of South American Earth Sciences 18, 11–25.

Selim, H.H., Yanik, G., 2009. Development of the Cambazlı (Turgutlu/MANISA) fissure-ridge-type travertine 744 and relationship with active tectonics, Gediz Graben, Turkey. Quaternary International 199, 157–163.

Shen, C.-C., Edwards, R.L., Cheng, H., Dorale, J.A., Thomas, R.B., Moran, S.B., Weinstein, S.E., Hirschmann, M., 2002. Uranium and thorium isotopic and concentration measurements by magnetic sector inductively coupled plasma mass spectrometry. Chemical Geology 185, 165–178.

Shen, C.-C., Cheng, H., Edwards, R.L., Moran, S.B., Edmonds, H.N., Hoff, J.A., Thomas, R.B., 2003. Measurement of attogram quantities of ^{231}Pa in dissolved and particulate fractions of seawater by isotope dilution thermal ionization mass spectroscopy. Analytical Chemistry 75, 1075–1079.

Shen, C.-C., Li, K.-S., Sieh, K., Natawidjaja, D., Cheng, H., Wang, X., Edwards, R.L., Lam, D.D., Hsieh, Y.-T., Fan, T.-Y., Meltzner, A.J., Taylor, F.W., Quinn, T.M., Chiang, H.-W., Kilbourne, K.H., 2008. Variation of initial ^{230}Th/^{232}Th and limits of high precision U–Th dating of shallow-water corals. Geochimica et Cosmochimica Acta 72, 4201–4223.

Shen, C.-C., Wu, C.-C., Cheng, H., Edwards, R.L., Hsieh, Y.-T., Gallet, S., Chang, C.-C., Li, T.-Y., Lam, D.D., Kano, A., Hori, M., Spötl, C., 2012. High-precision and high-resolution carbonate 230Th dating by MC-ICP-MS with SEM protocols. Geochimica et Cosmochimica Acta 99, 71–86.

Sierralta, M., Kele, S., Melcher, F., Hambach, U., Reinders, J., van Geldern, R., Frechen, M., 2010. Uranium-series dating of travertine from Süttö: implications for reconstruction of environmental change in Hungary. Quaternary International 222, 178–193.

Şimşek, Ş., 2003. Hydrogeological and isotopic survey of geothermal fields in the Büyük Menderes graben, Turkey. Geothermics 32, 669–678.

Şimşek, Ş., Günay, G., Elhatip, H., Ekmekci, M., 2000. Environmental protection of geothermal waters and travertines at Pamukkale, Turkey. Geothermics 29, 557–572.

Spötl, C., Vennemann, T.W., 2003. Continuous-flow isotope ratio mass spectrometric analysis of carbonate minerals. Rapid Communications in Mass Spectrometry 17, 1004–1006.

Sun, S., 1990. Denizli-Uşak arasının jeolojisi ve linyit olanakları (geology and lignite potential between Denizli and Uşak). Scientific report of the General Directorate of Mineral Research and Exploration of Turkey; No: 9985, Ankara, Turkey (in Turkish), p. 92.

Tan, O., Tapırdamaz, M.C., Yörük, A., 2008. The earthquake catalogues for Turkey. Turkish Journal of Earth Sciences 17, 405–418.

Tremaine, D.M., Froelich, P.N., Wang, Y., 2011. Speleothem calcite formed in situ: modern calibration of δ18O and δ13C paleoclimate proxies in a continuously-monitored natural cave system. Geochimica et Cosmochimica Acta 75, 4929–4950.

Utku, M., 2009. Etkinlik ve yığınsal etkinlik dönemlerine göre Denizli depremlerinin analizi. Maden Tetkik ve Arama Dergisi 138, 9–34 (in Turkish).

Uysal, I.T., Feng, Y., Zhao, J., Altunel, E., Weatherley, D., Karabacak, V., Cengiz, O., Golding, S.D., Lawrence, M.G., Collerson, K.D., 2007. U-series dating and geochemical tracing of late Quaternary travertine in co-seismic fissures. Earth and Planetary Science Letters 257, 450–462.

Uysal, I.T., Feng, Y., Zhao, J., Işık, V., Nuriel, P., Golding, S.D., 2009. Hydrothermal CO$_2$ degassing in seismically active zones during the late Quaternary. Chemical Geology 265, 442–454.

Van Noten, K., Claes, H., Soete, J., Foubert, A., Özkul, M., Swennen, R., 2013. Fracture networks and strike-slip deformation along reactivated normal faults in Quaternary travertine deposits, Denizli Basin, western Turkey. Tectonophysics 588, 154–170.

Wang, Y.J., Cheng, H., Edwards, R.L., An, Z.S., Wu, J.Y., Shen, C.C., Dorale, J.A., 2001. A high-resolution absolute-dated Late Pleistocene monsoon record from Hulu cave, China. Science 294, 2345–2348.

Wang, Y., Cheng, H., Edwards, R.L., Kong, X., Shao, X., Chen, S., Wu, J., Jiang, X., Wang, X., An, Z., 2008. Millennial- and orbital-scale changes in the East Asian monsoon over the past 224,000 years. Nature 451, 1090–1093.

Westaway, R., Guillou, H., Yurtmen, S., Demir, T., Scaillet, S., Rowbotham, G., 2005. Constraints on the timing and regional conditions at the start of the present phase of crustal extension in western Turkey, from observations in and around the Denizli region. Geodinamica Acta 18, 209–238.

Zhou, G.-T., Zheng, Y.-F., 2003. An experimental study of oxygen isotope fractionation between inorganically precipitated aragonite and water at low temperatures. Geochimica et Cosmochimica Acta 67, 387–399.